Plasma-activated water seed treatment modulates osmotic stress responses in pea through morphological, ionomic, hormonal, and antioxidant changes

Gábor Fejes[1,2], Tamás Bodor[1,2], András Kukri[1,2], Noémi Bába[1], Maria Gracheva[3,4], Ádám Solti[4], Ildikó Domonkos[5], Gyula Kajner[6], Ágnes Gallé[1], Réka Szőllősi[1,] Gábor Galbács[6], Kinga Kutasi[7], Zsuzsanna Kolbert[1]

[1] Department of Plant Biology, Faculty of Science and Informatics, University of Szeged, Közép fasor 52., H6726 Szeged, Hungary

[2] Doctoral School of Biology, Faculty of Science and Informatics, University of Szeged, Közép fasor 52., H6726 Szeged, Hungary

[3]Budapest Neutron Centre, Institute for Energy Security and Environmental Safety, HUN-REN Centre for Energy Research, Konkoly-Thege Miklós út 29-33., H1121 Budapest, Hungary

[4] Department of Plant Physiology and Molecular Plant Biology, ELTE Eötvös Loránd University, Pázmány Péter sétány 1/C, H1117 Budapest, Hungary

[5] Institute of Plant Biology, HUN-REN Biological Research Centre, Szeged, Hungary

[6] Department of Molecular and Analytical Chemistry, University of Szeged, Hungary

[7] Complex Fluid Research Department, Institute for Solid State Physics and Optics, HUN-REN Wigner Research Centre for Physics, Konkoly-Thege Miklós út 29-33., H1121 Budapest, Hungary

Gábor Fejes: gafej10@gmail.com

Tamás Bodor: szlon92@gmail.com

András Kukri: kukriandras2@gmail.com

Maria Gracheva: maria.gracheva@ek.hun-ren.hu

Ádám Solti: adam.solti@ttk.elte.hu

Ildikó Domonkos: domonkos.ildiko@brc.hu

Gyula Kajner: kajnerg@chem.u-szeged.hu

Ágnes Gallé: galle.agnes.anna@szte.hu

Réka Szőllősi: szoszo@bio.u-szeged.hu

Gábor Galbács: galbx@chem.u-szeged.hu

Kinga Kutasi: kutasi.kinga@wigner.hu

Zsuzsanna Kolbert: ordogne.kolbert.zsuzsanna@szte.hu

Abstract

Plasma-activated water (PAW) seed treatment is an emerging green technology that enhances plant germination and growth; however, its role in drought stress tolerance remains unclear. In this study, pea (*Pisum sativum* L.) seeds were treated with PAW (10 mg L^{-1} nitrite, 30 mg L^{-1} nitrate, pH 3.9), Zinc (Zn)-enriched PAW (PAW+Zn; 6 mg L^{-1} hydrogen peroxide (H_2O_2), 19 mg L^{-1} nitrite, 20 mg L^{-1} nitrate, 14 mg L^{-1} Zn, pH 4.7), distilled water (DW), or Zn-enriched DW. Subsequently, three-week-old plants were subjected to osmotic stress using polyethylene glycol 8000 (PEG8000) (20% w/v). PAW induced partial hilum opening and mild seed coat damage, while PA(W+Zn) increased nitric oxide (NO) accumulation. Both treatments enhanced nutrient levels and shootward translocation, particularly of Zn and iron (Fe). Under stress, PAW promoted the formation of larger but thinner leaves, indicating adaptive morphological responses. However, stomatal conductance, relative water content, photosynthesis, and starch accumulation remained unaffected. Unchanged proline levels and reduced soluble sugars suggest that classical osmotic acclimation was not induced by PAW treatments. Instead, both PAW and PA(W+Zn) increased abscisic acid (ABA) levels and *PsDHN2* expression, indicating activation of ABA-dependent stress signalling, likely mediated by nitrate-, nitrite-, and H_2O_2-derived signals. Tissue-specific cytokinin (CK) responses and enhanced antioxidant enzyme activities (superoxide dismutase [SOD], catalase [CAT]) further suggest the establishment of a primed state. Overall, PAW-based seed treatments induce complex physiological and molecular responses involving ABA signalling, selected ion translocation, and antioxidant enzymes without significantly improved water status, stomatal regulation, or photosynthetic performance.

Keywords: abscisic acid, cytokinin, nitric oxide, osmotic stress, pea, plasma-activated water, seed treatment

Introduction

Drought affects plant growth by inducing numerous morphological and physiological changes (Liao et al., 2025; Song et al., 2026). Drought has been reported to affect cell expansion, division and differentiation thereby influencing both plant growth (root, shoot and leaf growth, structure) and productivity in a direct manner. Furthermore, limited water supply disrupts key physiological processes in plants by impairing photosynthesis, reducing chlorophyll content, altering stomatal conductance and water relations. Drought disrupts both uptake and translocation of essential nutrients (e.g., zinc [Zn], iron [Fe], manganese [Mn]) in plants. Concurrently, it induces oxidative stress through excessive reactive oxygen species (ROS) accumulation, while plant tolerance depends on the efficiency of antioxidant defenses. In plants, drought-triggered ROS can be scavenged by antioxidant enzymes (e.g. superoxide dismutase [SOD], catalase [CAT], peroxidases [POD] etc.) and non-enzymatic antioxidants (e.g. ascorbate, glutathione, flavonoids). Another element of the internal defense processes of plants is the accumulation of compatible osmolytes (e.g., proline, soluble sugars) which maintain osmotic balance by lowering the osmotic potential, thereby facilitating water retention and preserving turgor pressure (Liao et al., 2025; Song et al., 2026). Drought stress responses are complemented by hormonal regulation, as phytohormones play a crucial role in initiating and modulating plant responses through a complex signalling network. Among these, abscisic acid (ABA) is a central regulator in drought-stressed plants. Elevated ABA levels induce stomatal closure, thereby reducing transpirational water loss, while also promoting the synthesis of compatible osmolytes and the expression of drought-responsive genes (e.g. Late Embryogenesis Abundant proteins, LEA) (Yoshida et al., 2014; Muhammad Aslam et al., 2022). Recently, the role of cytokinins (CKs) has also been recognized. CKs act antagonistically to ABA in the regulation of stomatal behaviour (Tanaka et al., 2006). Under drought conditions, CK levels typically decline in roots exposed to stress, which may promote root growth and contribute to a shift in the root-to-shoot ratio in favour of the root system (Ha et al., 2012).

In recent years, climate change has increased the frequency and severity of drought events, posing a major challenge to agriculture, driven by reduced precipitation and greater climatic variability (Verma et al., 2024; Biswas et al., 2025). To mitigate the adverse impacts of drought on crop production, the development and application of climate-smart technologies such as seed treatment/priming are essential (Saha et al., 2022). Pre-sowing seed treatment improves plant tolerance to both abiotic and biotic stresses by activating internal mechanisms, including enzyme activity, molecular signalling pathways, and antioxidant defense systems. Seed

treatment initiates early metabolic processes without inducing germination through controlled hydration enhancing germination rate, uniformity, and seedling vigour. As the treatment is applied exclusively to seeds, it also minimizes the release of chemicals into the environment (Thakur et al., 2022; Gohari et al., 2026). Sustainability is further improved by the seed-targeted application of reactive oxygen and nitrogen species (RONS)-containing plasma-activated water (PAW), which is produced without chemical additives. During plasma activation, a range of both short- and long-lived reactive species are generated in the liquid phase, including hydroxyl radicals (·OH), peroxynitrite ($ONOO^-$), nitrate (NO_3^-), nitrite (NO_2^-), hydrogen peroxide (H_2O_2), and ozone (O_3). During the creation of nitrate and nitrite from the gas phase nitric oxide (NO) and NO_2, or HNO_2 and HNO_3 (depending on the discharge and plasma-liquid system) (Lukes et al., 2014, Janda et al., 2025) dissolved into the water, the acidification of the water occurs, reaching pH values as low as 3 (Lukes et al., 2014). The acidic pH favours the recombination of nitrite through its reaction with H_2O_2 through the $NO_2^- + H_2O_2 + H^+ \rightarrow O{=}NOOH + H_2O$ process, leading to formation of short-lived peroxynitrite. Under acidic conditions the peroxynitrite's decomposition can occur through more routes, which can lead either to free OH· and NO_2· radicals, or to nitric acid immediately followed by dissociation into NO_3^- and H^+ (Lukes et al., 2014). As shown in our previous work (Kutasi et al., 2023) the pH of the PAW can be increased with the addition of metals, such as Zn, to the water to be treated, and thus mitigate the effect of the mentioned process during plasma treatment and storage. During the plasma treatment of water containing Zn solid surfaces, due to the oxidation-reduction reactions while the H^+ ions are reduced, the dissolution of Zn^{2+} ions occurs. In biological systems, Zn is central in determining protein structure and catalytic function in proteins like Zn-finger transcription factors, RNA polymerase, alcohol dehydrogenase, carbonic anhydrase, and Cu/Zn SOD (Stanton et al., 2022) thus influencing diverse developmental and stress response processes. Therefore, Zn supply in the liquid may also serve as beneficial micronutrient for the plants; however, the effects of Zn-supplemented PAW on plants remain largely unexplored. Furthermore, our knowledge is limited about the physiological, biochemical, and molecular pathways of plant osmotic stress responses modulated by seed-targeted PAW application.

Soil drought results in osmotic stress in plants, which is commonly and effectively mimicked in laboratory experiments by polyethylene glycol (PEG)-induced osmotic stress in nutrient solution systems (Michel & Kaufmann, 1973; Verslues et al., 2006). This study aimed to develop and characterize PAW with enhanced capacity to mitigate PEG-triggered osmotic stress

in pea plants *via* seed pre-treatment, and to elucidate for the first time the underlying regulatory mechanisms through which Zn-supplemented PAW may confer improved osmotic stress tolerance.

Materials and methods

1.1 Plasma-activated water

For the present study two types of PAWs were prepared: (i) PAW, obtained by plasma treatment of deionized water and (ii) PAWZn obtained by plasma treatment of deionized water containing Zn solid surface. The deionized water is produced with the ELGA Purelab Option-R 7 purifier and is characterized by Total Organic Carbon (TOC) < 20 ppb, Bacteria < 1 CFU/mL, resistivity > 15 MΩcm. The Zn has been used in powder form in order to enhance the solid surface and consequently the surface reactions. Zn powder, containing grains of irregular shape with sizes between 10 to 200 μm, was added to 32 ml water with a spoon of 0.0125 ml volume, corresponding to 17 mg (Kutasi *et al.* 2023). The powder was removed by filtration during its use in the seed treatment procedures.

The RONS were deposited into the water by using a surface-wave microwave discharge generated in a quartz tube of outer diameter 6 mm and inner diameter 4 mm, using as a main gas argon with 1% (v/v) addition of nitrogen and oxygen, respectively. The discharge has been ignited with an input power of 26 W using a CoberMuegge microwave generator (2450 MHz ±10 MHz, 300 W) based on magnetron (TO300-M23 Panasonic). The length of the discharge tube outside of surfatron body was 14 mm, and the gas flow rate was chosen to be 2 slm (standard liter per minute). These conditions have ensured the gas discharge plasma column to exceed the quartz tube (as shown in Figure S1), and the plasma plume outside the tube to be long enough (approx. 20 mm) to allow different contact points with the liquid surface, and as a consequence, the tuning of RONS concentration in the liquid phase (Kutasi et al., 2019). The 1% addition of N_2 and O_2 to Ar has been chosen to enhance the NO production in the discharge, while keeping the input power low (the molecular gases increase the power absorption, i.e. higher input powers are required to obtain the same length of plasma plume) and ensuring the stability of the discharge.

The main plasma species, which play role in the creation of RONS in the liquid phase are the electrons (contributing to the dissociation of H_2O and creation of H_2O_2), and the NO and NO_2 molecules, which initiate the formation of liquid phase nitrite and nitrate (Lukes et al., 2014). In the plasma plume, the electron density decreases, while the NO and NO_2 densities increase downstream (Kutasi et al., 2026). As a consequence, with increasing the distance between the discharge tube and the liquid surface the concentration of H_2O_2 is decreased, while that of the nitrate and nitrite is increased in the treated liquid (Kutasi et al., 2019, Bodor et al., 2026). In the present case the discharge tube-liquid distance has been chosen to be 15 mm, which resulted in nitrate/nitrite dominated PAWs.

The water was treated with the microwave discharge plasma for 10 min in a Berzelius beaker of 32 mL volume (as illustrated in Figure S1) placed on a magnetic stirrer (IKA lab disc, with the stirring speed set to 60-100 rpm). The water treatment was limited for 10 min in order to ensure that the final temperature of the water did not exceed 40-45 °C and the evaporation during treatment was negligible. The PAWs were transferred to Polypropylene (PP) containers and were handled and used for priming at room temperature.

The PAWs were characterized as described in (Kutasi et al., 2023). The compositions of PAWs are given in Table 1. As indicated by the table, the PAW contains only nitrate and nitrite, while the less acidic PAWZn contains additionally H_2O_2. In order to reactivate the reaction of NO_2^- with H_2O_2 under acidic conditions leading to peroxynitrite formation (the reaction kinetics is illustrated in Table 2 with the change of species concentrations during the 24 h priming), for seed priming the mixture of the one-day old PAW and PAWZn (50%-50% v/v), noting as PA(W+Zn), has been created and used immediately (noted as time = 0 h in Table 2). We note that the conductivity of the PAWs strongly depends on the pH (the evolution of the conductivities of different ion content PAWs have been analysed in detail in Kutasi et al. 2023).

Table 1. Characteristics of the prepared plasma-activated waters

Sample	**Ageing**	**[H_2O_2] [mg L^{-1}]**	**[NO_2^-] [mg L^{-1}]**	**[NO_3^-] [mg L^{-1}]**	**[Zn^{2+}] [mg L^{-1}]**	**pH**	**Conduc. [μS cm^{-1}]**
PAW	1 day	0	10±2	30±3	-	3.9±0.2	232±10
PAWZn	1 day	10±2	29±3	14±3	27.9±0.8	5.7±0.2	95±5

Table 2. Evolution of plasma-activated waters during the 24 h period of priming at room temperature.

Sample	time [h]	[H_2O_2] [mg L^{-1}]	[NO_2^-] [mg L^{-1}]	[NO_3^-] [mg L^{-1}]	[Zn^{2+}] [mg L^{-1}]	pH	Conduc. [μS cm^{-1}]
PAW	0	0	10±2	30±3	-	3.9±0.2	95±5
	24	0	7±2	32±3	-	3.9±0.2	95±5
PAW +seeds	0.1	0	10±2	30±3	-	4.9±0.2	n.a.
	1	0	10±2	30±3	-	5.1±0.2	264±10
	24	0	4±2	32±3	-	5.4±0.1	n.a.
PA(W+Zn)	0	6±1	19±2	20±3	14±0.8	4.7±0.1	138±5
	2	3±1	15±2	23±3	n.a.	4.7±0.1	140±5
	24	0	9±2	25±3	n.a.	4.6±0.1	145±5
PA(W+Zn) +seeds	0.1	6±1	19±2	20±3	14±0.8	5.1±0.1	n.a.
	1	5±1	18±2	22±3	n.a.	5.3±0.1	330±10
	24	0	8±2	20±2	n.a.	5.5±0.1	n.a.

1.2 Plant material, growth conditions, and experimental setup

The pea seeds (*Pisum sativum* L. cv Petit provencal, Rédei Kertimag Zrt.) were obtained from commercial markets. Seeds were sterilized with 5% (v/v) sodium hypochlorite for 20 minutes, followed by a 2-hour washing period in distilled water (DW), including two complete water replacements. After sterilization seeds were put into falcon tubes and the treating solutions were added onto them for 24h (1 mL/seed). The treatment solutions were the following: distilled water [DW], plasma-activated water [PAW], plasma-activated water with zinc [PA(W+Zn)], and zinc in distilled water [Zn]. After the 24h long pre-treatment seeds were put into petri dishes for 3 days in darkness. For each Petri dish, a sheet of filter paper was first placed at the bottom and moistened with 5 mL of DW. Eight seeds were then evenly distributed on the filter paper, covered with a second sheet of filter paper, and an additional 3 mL of DW was applied. The pre-germinated seeds were placed into vessels, four seeds in each container, supplied with a modified Hoagland solution (2 mM $Ca(NO_3)_2$, 1 mM $MgSO_4$, 0.5 mM KH_2PO_4, 0.5 mM Na_2HPO_4, 0.5 mM KCl, 10^{-6} M $MnSO_4$, 5×10^{-7} M $ZnSO_4$, 10^{-7} M $CuSO_4$, 10^{-7} M $(NH_4)_6Mo_7O_{24}$, 10^{-7} M $AlCl_3$, 10^{-7} M $CoCl_2$, 10^{-5} M H_3BO_3, 2×10^{-5} M Fe(III)-EDTA, pH 5.8)

and cultivated for 1 week, with the solution being replaced once halfway through the growth period. Finally, we established two experimental groups: one maintained in a standard control solution, and another subjected to osmotic stress by a 20 % (w/v) PEG 8000 solution (prepared with nutrient solution). Cultivation parameters in the greenhouse were the followings: photosynthetic photon flux density (PPFD) of 200 μmol m^{-2} s^{-1} supplied by white light-emitting diode (LED) lamps (5700 K), 12h light / 12h dark cycle, relative humidity between 55–60 %, and air temperature regulated at 24 ± 2 °C.

1.3 Seed surface structure analysis by scanning electron microscopy (SEM)

After the treatment, the seed coat was carefully removed, the region containing the hilum was excised, and this portion was subsequently dried for SEM analysis. The samples were mounted on SEM stubs, coated with 15 nm gold using a Quorum Q150T ES (Quorum Technologies, Lewes, UK) sputter and imaged in a JEOL JSM 7100F/LV (JEOL SAS, Croissy-sur-Seine, France) scanning electron microscope at 2 kV accelerating voltage. Hilum pore diameter was measured on the digital images using ImageJ Fiji (v.1.54g with Java 1.8.0_345). Spatial calibration was performed for each individual micrograph based on the pixel-to-micrometer ratio of the internal scale bar. To characterize morphological variability and account for irregularities in width along the hilar fissure, five local width measurements were obtained at representative locations distributed along the longitudinal axis of each hilum. The arithmetic mean of these measurements was then computed to derive the mean hilar diameter for each seed.

1.4 Microscopic analysis of NO and Zn ions in the seed coat

Segments from fresh pea seed coat were cut then fixed in 4 % (w/v) paraformaldehyde (PFA) solution according to the protocol of (Barroso et al., 2006). The tissues were embedded in a 5 % (w/v) agar matrix. Cross sections (100 μm thick) of embedded leaves were prepared with a vibratome (Zeiss-Microm, HM650V; Carl Zeiss, Jena, Germany), ensuring uniform and reproducible analysis among samples. NO levels in the seed coat cross-sections were semi-quantified by using 4-amino-5-methylamino-2′,7′-difluorofluorescein diacetate (DAF-FM DA), according to Kolbert et al., 2012, with slight modification. The segments were incubated in 10 μM DAF-FM DA solution for 60 minutes at room temperature in darkness. After the incubation period cross-sections were washed two times in Tris–HCl buffer (10 mM, pH 7.4).

For Zn level detection, 2-[[2-Methyl-8-[[(4-methylphenyl)sulfonyl]amino]-6-quinolinyl]oxy] acetic acid (Zinquin) probe was used (Helmersson et al., 2008). The seed coat cross-section

samples were incubated in 25 μM Zinquin solution (in 1x phosphate-buffered saline [PBS], pH 7.4) for 60 min at room temperature in darkness, followed by a single wash with PBS buffer prior to microscopic examination.

The fluorescently labelled seed coat cross-sections (in Tris–HCl buffer or 1x PBS, pH 7.4) were examined using Zeiss Axiovert 200M inverted microscope (Carl Zeiss, Jena, Germany), equipped with filter set 10 (exc.: 450–490 nm, em.: 515–565 nm) for DAF-FM DA and DAPI filter set (exc.: 365, em.: 455/50 nm) for Zinquin. Pixel intensities were quantified within circular regions (radius 48 μm) using the Zeiss Zen software (version 3.13; Carl Zeiss, Jena, Germany).

1.5 Analysis of nutrient distribution in seeds using X-ray fluorescence

The elemental distribution within the seeds was analyzed using X-ray Fluorescence (XRF) imaging after the samples were dried at 60 °C to an air-dry stage. XRF imaging was performed using a Horiba XGT7200V desktop XRF system equipped with a rhodium X-ray tube and a silicon drift detector. Energy calibration was achieved using a standard copper plate. The system operated under vacuum, applying an X-ray guide tube with a 100 μm diameter with voltage set to 50 kV and current of 1 mA. Mapping areas of 11.3 mm x 11.3 mm for seeds and 4.1 mm x 4.1 mm for coats were measured with a survey time of 1500 s per frame, collecting the data 3 times per pixel. The distribution of Zn was analyzed by detecting the characteristic Kα 1 photons, which have a peak energy at approximately 8.616 keV. Data analysis and representation were performed using the multi-dimensional data analysis package Hyperspy (1.7.5) (de la Peña et al., 2022) in Python 3.11. Distribution profiles were calculated by averaging the normalized pixel values within defined Regions of Interest (ROIs) using the ImageJ Fiji software (v.2.16.0/1.54p with Java 1.8.0_322).

1.6 Biomass measurements in vegetative-stage pea plants

Parameters reflecting biomass production were assessed on harvest. Shoot and root length were measured using a graduated ruler. Leaf area was quantified using ImageJ software (v.1.54g with Java 1.8.0_345; National Institutes of Health, Bethesda, MD, USA) based on digital images. Fresh, dry and turgid weights were quantified using an analytical balance with a measurement accuracy of 0.001 g. Leaf relative water content (RWC) was calculated based on the following equation:

$$RWC\ \% = \frac{\text{fresh weight} - \text{dry weight}}{\text{turgid weight} - \text{dry weight}} * 100$$

1.7 Microscopic analysis of the leaf tissue structure

Leaf segments were prepared as described in 1.4. The leaf cross-sections (in 1x PBS, pH 7.4) were examined using bright-field microscopy (Zeiss Axiovert 200M, Carl Zeiss, Jena, Germany). Anatomical parameters (whole leaf blade thickness, mesophyll layer, palisade layer, spongy layer, ratio of palisade/spongy layers) were measured by using Zeiss Zen (version 3.13) software (Carl Zeiss, Jena, Germany).

1.8 Analysis of microelement concentrations using ICP-MS in root and shoot system of pea

All inductively coupled plasma mass spectrometry (ICP-MS) analyses were carried out on an Agilent 7700x ICP-MS system (Agilent, Santa Clara, USA) fitted with an Agilent I AS autosampler. The plasma torch was run with an argon gas flow of 15 L min^{-1} and an R.F. forward power of 1550 W. The sample uptake rate, nebulizer gas flow, and sampling depth were adjusted to 750 mL min^{-1}, 1.05 L min^{-1}, and 10 mm, respectively. All experiments were performed using Agilent MassHunter software for instrument control and data acquisition (Agilent, Santa Clara, CA, USA). Data acquisition was carried out in analogue mode with a uniform integration time of one second, applied to all monitored isotopes (^{11}B, ^{23}Na, ^{24}Mg, ^{39}K, ^{44}Ca, ^{45}Sc, ^{55}Mn, ^{56}Fe, ^{58}Ni, ^{59}Co, ^{63}Cu, ^{66}Zn, ^{78}Se) and for both tuning conditions (No Gas, He). Signals for all isotopes were recorded in No Gas tune mode, except for ^{44}Ca, ^{56}Fe and ^{78}Se, where Agilent ORS3 collision cell (He mode) was used to reduce the effect of spectral interferences. The dried leaf and root material were digested in a solution consisting of 6 mL concentrated nitric acid (HNO_3) and 2 mL concentrated H_2O_2, after which the volume was brought up to 20 mL with DW. The digested samples were subjected to an 83.3-fold dilution and subsequently fortified with scandium at a concentration of 10 ppb, serving as the internal standard. The ICP-MS instrument was run with high-purity argon (99.996%) and helium (99.999%) gases, both supplied by Messer Hungarogáz kft. (Budapest, Hungary). All samples were prepared using trace-analytical purity de-ionized water obtained from a MilliPore Elix 10 device equipped with a Synergy polishing unit (Merck GmbH, Rahway, Germany). Calibration standards were prepared from the Inorganic Ventures IV-ICPMS-71A multielement stock solution. Elements used as internal standards were added to all solutions using Inorganic Ventures IV-ICPMS-71D six-element ICP-MS internal standard stock solution (Inorganic Ventures, Christiansburg, USA).

Translocation factors were calculated according to the following equation (Eid and Shaltout, 2016):

$$\mathrm{TF} = \frac{\text{element concentration in shoot tissues (ppm)}}{\text{element concentration in root tissues (ppm)}}$$

1.9 Determination of stomatal conductance and stomatal density

Stomatal conductance (g_s) was measured on the surface of fully developed, undamaged leaves using a steady-state diffusion porometer (PMR-2 Steady state porometer, PP Systems, Amesbury MA, USA). Measurements were conducted between 10:00 and 12:00 h to encompass the interval of peak stomatal opening. Data were expressed in mmol m^{-2} s^{-1}. Plant leaves were immersed in MES/KCl buffer (10/50 mM, pH 6.15), and the epidermal layers were gently peeled off with forceps. In all cases, the epidermal strips were taken from the same region of the leaf blade, avoiding the veins. The epidermal layers were then mounted on slides in the same buffer. Images were captured with a Zeiss Axiovert 200 M microscope and processed using Zeiss Zen (version 3.11) software. Stomatal density (pieces/mm^2) was determined by counting all stomata within a circle of 200 µm in radius. For stomatal aperture measurements, the widths of the stomatal pores were recorded (data not shown).

1.10 Measurement of ABA and proline concentrations

For the quantification of ABA content of pea leaves, a colorimetric ABA ELISA kit (Antibodies-online GmbH, ABIN6973585) was used according to the manufacturer's instructions (Luo et al., 2016; Cheng et al., 2018). For the proline assay, a modified protocol based on (Bates et al., 1973) and (Magné and Larher, 1992) was used. Samples were ground in liquid nitrogen, followed by the addition of 3% (w/v) sulfosalicylic acid, after which they were centrifuged at 3824 x g for 15 minutes, and the resulting pellet was subsequently discarded. A 0.5 mL sample was combined with 2 mL of 1% (v/v) ninhydrin solution (prepared in 60:40 v/v glacial acetic acid:distilled water) and then incubated at 100 °C for 1 hour. After the incubation the reaction was terminated on ice. Five milliliters of toluene (≥99.5 %) were added to each test tube, after which the mixture was vigorously shaken. Following complete phase separation, the absorbance of the upper (organic) phase was measured at 520 nm using JASCO V-730 UV-Visible Spectrophotometer (JASCO UK).

1.11 Determination of leaf pigments and chlorophyll fluorescence

Leaf discs (25 mg) were collected from independent plants, and three biological replicates were taken from each treatment. They were homogenized in 1 mL of pure acetone and then incubated in a refrigerator for 24 hours. Following incubation, the samples were centrifuged at 22540 x g for 15 minutes at 4 °C. The supernatant was collected, after which 1 mL of 80% (v/v) ethanol (prepared in 10 mM TRIS, pH 7.8) was added to the pellet and incubated for 24 h. Following an additional centrifugation step, the resulting supernatants were combined, and their absorbance was recorded at 663, 650, 647, 537, 529, and 470 nm using JASCO V-730 UV-Visible Spectrophotometer (JASCO UK), respectively. Data analysis conducted in accordance with the methodology described by (Sims and Gamon, 2002).

The maximum quantum efficiency of Photosystem II (PSII) ($F_v/F_{m)}$ was determined by using a chlorophyll fluorometer FluorPen FP 110 (Photon Systems Instruments, Brno, Czech Republic).

1.12 Quantification of glucose, sucrose and starch contents in pea leaves

A total of 200 mg of leaf tissue was ground in liquid nitrogen, after which 100 mg of the homogenate was combined with 1 mL of 80 % (v/v) ethanol and heated at 80 °C for 30 min. The solution was centrifuged at 2550 x g for 10 minutes. A second extraction step was then performed, and the resulting supernatants were collected and later used for soluble sugar quantification. To the pellet obtained previously, we added 1 mL of ultrapure water and centrifuged again at 2550 x g for 10 minutes. After this step, the supernatant was removed, and 1.1% (v/v) hydrochloric acid was added to the pellet, followed by incubation at 100 °C for 30 minutes. Finally, the samples were centrifuged at 2550 x g for 10 minutes. The resulting supernatant was collected and used for starch content determination. All samples were diluted and made into three technical replicates. To each test tube, 2.5 mL of ice-cold 72 % (v/v) sulfuric acid containing 10 mM anthrone (97%) was added. The mixtures were vortexed thoroughly and then incubated at 95 °C for 8 minutes. The absorbance of the samples was measured at 630 nm in spectrophotometer (KONTRON, Milano, Italy). For soluble sugars, 80% (v/v) ethanol was used as the blank, while for starch, the blank consisted of 1.1% (v/v) hydrochloric acid (Hansen and Møller, 1975).

1.13 Measurement of SOD, CAT and POD activities in pea leaves

To determine the activities of SOD, CAT, and POD, 200 mg of fully developed leaves were harvested and ground in a phosphate buffer (100 mM, pH 7.0) containing 1% w/v polyvinylpolypyrrolidone and 1 mM phenylmethylsulfonyl fluoride to block protease activity (Tari et al., 2015). The resulting extract was transferred to a microcentrifuge tube and centrifuged at 12,000 × g for 20 minutes at 4°C. SOD (EC 1.15.1.1) activity was quantified spectrophotometrically using the change in NBT coloration as the indicator. In this assay, one unit of SOD is defined as the enzyme quantity that inhibits NBT reduction by 50% (Dhindsa et al., 1981). CAT (EC 1.11.1.6) activity was determined based on its ability to decompose H_2O_2 into water and oxygen, monitored as a decrease in absorbance at 240 nm. One unit of CAT is defined as the amount of enzyme that decomposes 1 μmol of H_2O_2 per minute (Upadhyaya et al., 1985). POD (EC 1.11.1.7) activity was assessed by monitoring the rise in absorbance caused by guaiacol oxidation. One unit of guaiacol is defined as the quantity of enzyme that generates 1 μmol min^{-1} of oxidized guaiacol (Horváth et al., 2015). In every instance, a JASCO V-730 UV-Visible Spectrophotometer (JASCO UK) was employed.

1.14 RT-qPCR analysis of osmotic stress- and CK-related genes

For gene expression analysis, tissue from three individual plants was ground in liquid nitrogen, and total RNA was subsequently isolated using a Quick-RNA™ Miniprep Kit (Zymo Research, Irvine, CA, USA). The quality of the isolated RNA was assessed with a Titertek-Berthold (Berthold Detection Systems GmbH, Germany) Colibri Microvolume Spectrometer. Samples with sufficient quality were reverse transcribed into cDNA with random hexameric (Esco Micro Pte. Ltd AERIS-BG096, Singapore) using MMLV reverse transcriptase (Thermo Scientific, Waltham, MA, USA). Relative gene expression levels were then evaluated by real-time quantitative Polymerase Chain Reaction (RT-qPCR) using a qTOWER 2.0 system (Analytik Jena, Jena, Germany). The target and reference genes were sourced from the National Center for Biotechnology Information (NCBI; https://www.ncbi.nlm.nih.gov/). Each individual RT-qPCR reaction consisted of 5 μL Maxima SYBR Green qPCR Master Mix (2×) (Thermo Scientific, Waltham, MA, USA), 3 μL molecular biology grade water (Thermo Scientific, Waltham, MA, USA), 10 ng cDNA, and primers at a final concentration of 400–400 nM The RT-qPCR protocol started with an initial denaturation step at 95°C for 7 minutes, followed by 40 amplification cycles consisting of denaturation at 95°C for 15 seconds and a combined annealing/extension phase at 60°C for 1 minute. After the amplification reactions were

completed, the generated data were evaluated with the RT-qPCR instrument's dedicated software (qTOWER Software 2.2; Analytik Jena, Jena, Germany) (Kukri et al., 2024) and relative gene expression levels were determined by the 2(-ΔΔCt) method (Livak and Schmittgen, 2001). The genes examined were the following: *PsERD1, PsARR5, PsARR9, PsARR17, PsAHK3, PsAHK4, PsRD20, PsP5CS, PsDHN2, PsDREB2A*. For reference we used *PsPP2A*. Primers are listed in Table S1.

1.15 Statistical analysis

All experiments were conducted at least twice using independent biological generations. To ensure statistical rigor and avoid pseudoreplication, each treatment group per generation consisted of three independent vessels, with each vessel containing four plants. For morphological and growth parameters (e.g., root and shoot length, biomass), measurements from all plants within a single vessel were averaged, and this vessel mean was treated as the primary experimental unit for the analysis. For biochemical assays (e.g., SOD activity, proline, and soluble sugar content), three technical replicates were measured per sample to ensure analytical precision and subsequently averaged into a single value for each biological unit. Statistical analyses were performed using OriginPro 2021 software (OriginLab Corporation, Northampton, MA, USA). One-way ANOVA was applied for seed coat stainings, XRF, and leaf thickness. In the specific case of leaf thickness, one-way analysis was chosen because these measurements focused on comparing the effects of different seed treatments specifically under PEG-induced stress conditions, relative to the absolute DW control. For parameters involving both seed treatment and osmotic stress, a two-way ANOVA was performed to evaluate the main effects of 'Seed Treatment' (DW, PAW, PA(W+Zn), and Zn) and 'Osmotic Stress' (0 and 20 w/v% PEG8000), as well as their interaction. All ANOVA tests were followed by Tukey's post-hoc test for multiple comparisons with a significance threshold of $P < 0.05$. Different letters indicate statistically significant differences among all treatment combinations at $p < 0.05$ according to Tukey's post-hoc test. To account for possible variability across independent experimental runs, "experimental generation" was initially incorporated as a blocking factor in the ANOVA model. Because this blocking effect was not statistically significant ($P > 0.05$), data from the separate generations were pooled for the final factorial analysis to enhance statistical power. The data are presented as the mean ± standard error (SE).

2. Results and discussion

Seed-stage effects of PAW pre-treatments: hilum and seed coat structure, nutrient homeostasis

In pea seeds, the hilum region has a role in water absorption and germination initiation, functioning as a hygroscopic valve (Upretee et al., 2024). Compared to the normal hilum structure of the DW-soaked seed, Zn and PA(W+Zn) treatments caused slightly more opened fissure. The trachea within the fissure exhibited a slight loosening in DW, PA(W+Zn) or Zn treated seeds. Compared to DW seed, PAW led to a statistically significant opening of the fissure, which was accompanied by a pronounced loosening of the trachea (Fig. 1, Fig. S2). Moreover, the surface of DW-soaked seeds and Zn-treated seeds near the hilum appeared smooth possibly due to its intact cuticle layer, while PAW treatment resulted in rougher seed surface (suggested by the qualitative observation of surface damage in Fig. 1 BC, indicated by arrows) possibly due to the loss of the hydrophobic wax layer. Consistent with these findings, previous studies have shown that PAW can oxidize and remove surface lipids, thereby facilitating water uptake (Billah et al., 2020; Rathore et al., 2021; Than et al., 2021; Gone and Singh, 2025). These indicate that the observed effects on the hilum size and the seed surface adjacent to the hilum are mainly PAW (~pH 4)-specific and may be attributed to acidification-induced changes (e.g. protonation of pectins, weakening of calcium-mediated cross-links) in seed coat cell wall properties. However, primarily hilum opening is a consequence of imbibition-induced swelling, low pH may possibly modify cell wall structure to intensify loosening. An enlarged hilum aperture may enhance water uptake, thereby facilitating germination processes.

To assess the immediate impact of seed treatments on the seed coat, levels of NO and Zn ion were semi-quantified using microscopy. In seed coat sections, PA(W+Zn) treatment resulted in significantly elevated (377%) NO levels relative to the control (Fig. 2A and C). Seed treatment with Zn did not affect NO levels of the seed coat. PA(W+Zn) solution contains H_2O_2 and its nitrite content is enhanced, while $ONOO^-$ formation can also take place. Nitrite acts as a direct NO source, as its reduction in the presence of ascorbate at acidic pH can spontaneously generate NO (Wang and Hargrove, 2013). In addition, the conversion of nitrite to NO may occur via nitrate reductase (NR), either through direct (Rockel et al., 2002; Mohn et al., 2019) or indirect mechanisms (Stöhr et al., 2001; Chamizo-Ampudia et al., 2017). Additionally, H_2O_2 being present in PA(W+Zn) may also be responsible for NO formation *via* mitogen activated protein kinase 6-mediated phosphorylation of NR enzyme (Wang et al., 2010). Interestingly, Zn-

associated fluorescent signals were unchanged by PAW, PA(W+Zn) and even by Zn treatment compared to the control (DW) (Fig. 2B and D). Zinquin is a fluorescent probe that detects labile, loosely bound Zn^{2+} pools rather than total cellular Zn in plant tissues; accordingly, the lack of increased fluorescence following Zn seed treatment suggests that the applied Zn did not enhance the labile Zn^{2+} pool in the seed coat, but was likely sequestered by cell wall components such as pectins, proteins, phenolics, or phytate (Khotimchenko et al., 2008; Kalinowska et al., 2020; Marolt et al., 2020).

To evaluate the possible effect of the treatments on the seed nutrient profile, macro- and microelement distributions were detected in the treated seeds by XRF spectroscopy (Fig. 3AB). Zn levels were elevated by all treatments relative to DW, with the PA(W+Zn) and Zn treatments exhibiting the highest and statistically most significant increases (199% and 218% compared to DW, respectively) due to direct Zn supply. The acidic nature of PAW (pH ~4) may enhance Zn accumulation in seeds by releasing Zn from binding sites into a more labile, bioavailable pool. In case of Fe and Ca, only the PAW treatment caused significantly elevated content probably due to low pH-induced increase in mobilization and solubilization. The changes in Mn, Cl, and S levels showed comparable patterns, with the Zn treatment resulting in significant increase compared to DW. The observed increase in Mn, Cl, and S levels in seeds following Zn treatment may reflect Zn-induced modulation of metal and anion transport, ion homeostasis, and metabolic demand, resulting in enhanced accumulation of these elements in the seed tissue. Ni exhibited elevated concentrations following treatment with PAW or Zn, while Na content was increased only by the PA(W+Zn) treatment. K content increased in response to PAW treatment and showed a further increase under Zn treatment (Fig. 3AB). Consequently, the *in-seed* levels of key macro- and microelements is enhanced potentially improving germination performance and stress resilience by facilitating early metabolic activation.

PAW seed treatments influence leaf growth in osmotic stressed pea

Following the seed-stage, the effect of seed treatments on unstressed and osmotic stress-affected vegetative-stage pea plants were evaluated (Fig. 4). None of the seed treatments affected the root and shoot growth parameters of the plants under control conditions. Osmotic stress did not change the number of lateral roots (Fig. 4C) and shoot length (Fig. 4D) based on pairwise comparisons, but according to two-way ANOVA, PEG stress had a significant effect on shoot length ($p = 1.78 \times 10^{-7}$) and lateral root length ($p = 1.17 \times 10^{-88}$). Osmotic stress significantly

reduced the length of primary and lateral roots (Fig. 4AB) and leaf area (Fig. 4EF) in DW plants compared to plants under normal osmotic conditions. These indicate that root cell elongation and leaf cell expansion are the most osmotic stress-sensitive cellular processes (González-Bernáldez et al., 1968; Lecoeur et al., 1995). Of the parameters examined, only leaf area showed notable increase as the effect of PAW and PA(W+Zn) seed treatments compared to DW under osmotic stress. PAW and PA(W+Zn) resulted in 34% and 33% increases compared to DW under osmotic stress, which resulted in leaf area similar to that of the healthy plants (Fig. 4EF). This effect was supported by the significant interaction between seed treatment and osmotic stress on leaf area ($p=0.0284$) accoriding to two-way ANOVA. The ability of PAW and PA(W+Zn) seed treatments to fully restore leaf area under osmotic stress, without affecting growth under control conditions, indicates an effective long-term priming mechanism that selectively enhances shoot resilience. Similarly, significant induction of leaf growth was observed in pea plants developed from PAW-soaked seeds (Dahal et al., 2024). Additionally, notable increase in foliar area was detected in non-stressed lettuce and tomato irrigated with PAW, and the inducing effect was linked to the nitrate content of PAW (Stoleru et al., 2020; Than et al., 2021; Priatama et al., 2025). The growth habit of control and seed treated pea plants is shown in Fig. S3.

To further investigate PAW effects in leaves, anatomical traits such as total leaf blade thickness, mesophyll thickness, palisade layer thickness, spongy layer thickness were determined using optical microscopy (Fig. 5). PEG8000-associated osmotic stress significantly reduced all anatomical parameters in the leaf of DW treated plants, indicating inhibited cell expansion and/or cell number. Interestingly, under osmotic stress, seed treatments with PAW and Zn led to additional reductions in the thickness of the leaf blade, mesophyll, and spongy layers, with the most pronounced effect observed for Zn (Fig. 5AB). The ratio of spongy and palisade layers was not influenced by the treatments (data not shown). In case of Zn seed treatment, both leaf area and leaf thickness are reduced by osmotic stress indicating an overall negative effect on leaf size. In contrast, PAW seed treatment resulted in larger but thinner leaves, suggesting a possible adjustment in leaf morphology that could influence light interception and construction cost per unit leaf area, although further experiments are required to substantiate this interpretation.

PAW seed treatments modify concentrations and interorgan translocation of micronutrients in osmotic stress-exposed pea

The possible changes in nutrient distribution underlying growth responses were studied by measuring *in planta* concentrations of microelements and calculating translocation factors (Table 3AB). Translocation factors were additionally calculated based on total elemental content (shoot/root), providing a biomass-weighted estimate of elemental partitioning between organs (Table S3). In the leaves of unstressed plants, the PAW, PA(W+Zn) and Zn seed treatments increased Zn concentration (Table 3, Table S3). For the Zn-containing treatment solutions, the observed increase in leaf Zn concentrations indicates that seed-applied Zn remains bioavailable and is efficiently translocated to the aerial tissues during subsequent developmental stages. In the case of Fe, both the PAW and Zn seed treatments caused an increase, while B, Cu and Ni concentrations did not change significantly compared to DW under normal water supply. Mn, similarly to Zn, showed an increase in the leaves of the healthy plants due to PAW, PA(W+Zn) and Zn seed treatments. Overall, these results demonstrate that seed treatments with PAW and Zn have long-term effects on plant nutrient status, as reflected by increased Zn and Mn concentrations in leaves under non-stress conditions. Furthermore, the ability of PAW to enhance Zn, Mn, and Fe accumulation suggests that PAW-induced modifications during germination may improve nutrient mobilization and uptake capacity, likely through modulation of metal transport and homeostasis pathways. In the leaves of DW plants, the osmotic stress significantly reduced the concentrations of all measured micronutrients except Zn which can partly be responsible for growth reductions (see Fig. 4 A,B,E,F). The reduction in leaf micronutrient concentrations under osmotic stress can be explained by decreased water uptake and transpiration-driven mass flow, coupled with impaired root uptake capacity and reduced translocation to the shoots (da Silva et al., 2011; Naik et al., 2022). Zn-containing treatments [PA(W+Zn) and Zn] under osmotic stress led to leaf Zn concentrations exceeding those of unstressed plants, indicating enhanced Zn uptake and translocation and highlighting a strong priming effect on Zn homeostasis. In Fe concentrations, which were reduced by osmotic stress, both PAW and Zn seed treatments resulted in a significant increase compared to DW. The leaf Fe concentration created by the PAW seed treatment was similar to that of the healthy plant. Additionally, B concentrations were increased by PAW and PA(W+Zn) compared to DW under osmotic stress, but the resulted B levels were much lower compared to non-stressed DW plants. Interestingly, Mn and Cu concentrations, which were reduced by osmotic stress, were not improved by the seed treatments. In Ni concentrations, the PAW treatment resulted in a 10-fold increase under osmotic stress, but this only increased the Ni content to one third of the Ni content of the healthy leaf (Table 3A, Table S3). The differential response of micronutrients to seed treatments under osmotic stress suggests

that PAW primarily enhances the mobilization and translocation of selected elements such as Fe, B, and Ni, likely through acidification- and redox-driven processes, whereas tightly regulated elements such as Mn and Cu remain unaffected. This highlights the element-specific nature of stress mitigation and nutrient homeostasis in treated plants.

In the root system of unstressed pea, Zn contents were slightly, and Fe and Mn contents were notably increased by PAW, PA(W+Zn) and Zn seed treatments, while B, Cu and Ni concentrations were not significantly affected (Table 3B, Table S3). Similar to the leaves, in the root system of DW plants, osmotic stress caused relevant decrease in the concentrations of all measured microelements. All seed treatments further reduced Zn and Fe concentrations in the root, but did not affect Mn, Cu and Ni contents. The B content of the root, which was significantly suppressed by osmotic stress, was increased by the PAW and PA(W+Zn) treatments (Table 3B, Table S3). The reduction of Zn and Fe concentrations in roots of seed-treated plants under osmotic stress, coupled with their increased accumulation in leaves, indicates enhanced root-to-shoot translocation driven by seed treatments. The extent of element translocation from the root to the shoot was determined by calculating the translocation factors (Table 3A, Table S3). Under normal osmotic conditions, there was no significant difference in the root-shoot translocation of elements due to seed treatments. Osmotic stress significantly increased the transport of B and Ni into the shoot, and to a lesser extent increased the transport of Zn, Mn and Cu, but did not affect the distribution of Fe. In plants exposed to osmotic stress, PAW seed treatment significantly increased the transport of Zn and Fe into the shoot. Additionally, in the case of Zn, both PA(W+Zn) and Zn seed treatments resulted in an increase in the translocation factor value compared to DW. In the case of B, the increased translocation towards the shoot triggered by osmotic stress was reduced by the PAW and PA(W+Zn) seed treatments. The translocation of Ni, Cu and Mn was not significantly affected by seed treatments in plants exposed to osmotic stress and DW seed treatment (Table 3A, Table S3). The similar effect of seed treatments suggests that no PAW-specific modulatory effect can be identified regarding nutrient homeostasis and distribution.

PAW seed treatments induce ABA but has limited effect on proline accumulation in osmotic stress-exposed pea

To further explore the targets of PAW-related effects in pea, additional leaf-specific osmotic stress responses were studied. The stomatal conductance values of PAW, PA(W+Zn) or Zn

seed-treated plants did not differ from those measured in DW plants under normal osmotic conditions. Osmotic stress notably reduced stomatal conductance, which was not statistically significantly modified by seed treatments compared to DW (Fig. 6A). Similary, no significant differences in the sizes of stomatal apertures were determined by microscopic observation of epidermal peels of PAW, PA(W+Zn) or Zn seed-treated plants compared to DW plants under osmotic stress (data not shown). These reflect that seed treatments did not further decrease stomatal conductance under osmotic stress. Adaxial stomatal density was significantly increased by PA(W+Zn) under stress-free conditions (without affecting leaf area, Fig. 2EF) suggesting a direct effect on stomatal development rather than a size-related artefact. Osmotic stress increased stomatal density on the adaxial side, which was significantly reduced by PAW and PA(W+Zn) treatments (Fig. 6C). Two-way ANOVA revealed a significant interaction between seed treatment and osmotic stress on adaxial stomatal density ($p = 6.4 \times 10^{-12}$). These effects may be attributable to changes in leaf area (see Fig. 4 EF). On the abaxial side, stomatal density did not change with the treatments or stress according to the post-hoc Tukey's test (Fig. 6D); however two-way ANOVA revealed a significant interaction between seed treatment and osmotic stress ($p = 0.03581$) suggesting that the treatments induced a coordinated, but subtle, modification of the abaxial leaf surface architecture in response to PEG stress. RWC of the leaves decreased in osmotic stress-exposed DW plants. The PAW and PA(W+Zn) treatments slightly (non-significantly) increased the RWC, while Zn seed treatment caused a significant elevation compared to DW (Fig. 6B). ABA content was slightly (non-significantly) increased by osmotic stress treatment in the DW leaves, while PAW and PA(W+Zn) seed treatments caused a further, statistically significant increase in ABA content (Fig. 6E). Additionally, ABA content remained low in the leaves of Zn seed-treated, osmotic stressed plants indicating PAW-specific induction of the ABA content in osmotic-stressed exposed pea. Two-way ANOVA confirmed a highly significant interaction between seed treatment and osmotic stress for ABA accumulation ($F = 13.47$, $p = 0.00171$). At the same time, PAW- and PA(W+Zn)-induced ABA accumulation was not accompanied by a further decrease in stomatal conductance (Fig. 6A). This apparent discrepancy may be explained by the fact that osmotic stress itself already strongly reduced stomatal aperture, thereby limiting the extent of further closure. Moreover, stomatal behaviour is regulated not only by ABA levels but also by hydraulic signals, ROS/NO signaling, guard cell sensitivity, and temporal dynamics of the stress response. As for proline, osmotic stress increased its amount in DW leaves suggesting the activation of osmoprotective mechanisms in pea (Fig. 6F). Two-way ANOVA revealed significant effects of treatment ($F = 4.86$, $p = 0.0044$), PEG stress ($F = 107.47$, $p < 0.001$), and their interaction ($F = 7.05$, $p < 0.001$)

on proline content. Under non-stress conditions, only minor differences were observed among treatments, whereas under PEG stress, Zn treatment induced the highest proline accumulation according to Tukey's post hoc test ($p < 0.05$). The significant interaction between treatment and stress ($p < 0.001$) confirms that seed priming did not merely increase proline levels overall, but specifically modulated the plant's metabolic adjustment to osmotic challenges. This demonstrates that PAW and Zn-supplemented PAW treatments act as effective priming agents, preparing the proline biosynthetic pathway for a more robust response upon encountering stress. Similar to our results, foliar application of PAW doesn't trigger proline accumulation in barley (*Hordeum vulgare*, Bussmann et al., 2023). However, it was recently reported that PAW increased proline content in drought-stressed *Poa pratensis*; notably, this effect was observed under a combined treatment regime involving both seed priming and PAW irrigation (Zaboli et al., 2025).

Limited effects of PAW seed treatments on osmotic stress-induced changes in leaf pigments and PSII efficiency

As an additional leaf-specific process, we examined the light phase of photosynthesis and the related pigment composition of the leaves. Osmotic stress significantly affected carotenoid ($p = 4.25 \times 10^{-4}$) and anthocyanin ($p=0.0046$) (Fig. 7B and C, respectively) contents according to two-way ANOVA; however, post hoc comparisons revealed only modest differences among individual groups. Chlorophyll content was primarily affected by PEG-induced osmotic stress ($p=6.36 \times 10^{-10}$, Fig. 7A), while treatment effects and the interaction ($p=0.05295$) remained statistically non-significant. The slightly changed carotenoid and anthocyanin levels, together with increased chlorophyll content, suggest that the applied osmotic stress treatment did not induce a strong photoprotective pigment response but may have altered chlorophyll accumulation or turnover. The changes caused by osmotic stress in the DW were not influenced by the PAW, PA(W+Zn) or Zn seed treatments (Fig. 7ABC). Osmotic stress significantly decreased F_v/F_m, suggesting damage to PSII photochemistry in DW plants. Two-way ANOVA confirmed significant effects of both seed treatment ($p=0.0165$) and PEG-induced osmotic stress ($p=3.12\times10^{-14}$) on F_v/F_m, while the interaction effect showed borderline significance ($p=0.0546$). However, post hoc comparisons revealed only modest differences among individual treatment groups under osmotic stress. Although PAW seed treatment resulted in a slight, non-significant improvement, PA(W+Zn) and Zn treatments did not markedly alter F_v/F_m

values (Fig. 7D), suggesting that these treatments did not primarily target PSII stability or repair mechanisms. Through foliar application, PAW doesn't improve chlorophyll levels and quantum yield of PSII in barley (Bussmann et al., 2023). Contrast with this and our findings, some experimental systems have reported that PAW seed treatments can enhance pigment content and/or photosynthesis under drought stress; however, these studies involved either combined PAW seed and irrigation treatments (Zaboli et al., 2025) or direct cold plasma treatment of seeds (Li et al., 2025).

PAW seed treatments decrease osmotic stress-induced sugar accumulation in pea leaves

The glucose and sucrose content increased under osmotic stress in the leaves of DW plants (Fig. 8AB). The increased glucose and sucrose contents under osmotic stress suggest that –besides proline accumulation (Fig. 6F) - DW plants also mobilize soluble sugars to maintain osmotic balance and to support cellular protection mechanisms (Mohammadi Alagoz et al., 2023). PAW and Zn seed treatments markedly decreased the accumulation of glucose and sucrose under osmotic stress, likely reflecting enhanced sugar allocation toward the biosynthesis of protective compounds. Although the effect of PA(W+Zn) was weaker and not statistically significant in pairwise comparisons (Fig. 8AB), two-way ANOVA revealed significant treatment × stress interactions for both glucose ($p=0.00127$) and sucrose ($p=0.00193$), indicating that the effects of seed treatments on soluble sugar accumulation were strongly dependent on osmotic conditions. While Zaboli et al., (2025) combined PAW seed priming with irrigation in *Poa pratensis*, and observed enhanced soluble sugar accumulation under drought, our study applied PAW only as a seed treatment in pea, likely insufficient to elicit the same response. Additionally, starch content of the leaves was not significantly affected by either osmotic stress or seed treatments (Fig. 8C). The stability of leaf starch levels suggests that osmotic stress and the applied seed treatments primarily influenced soluble sugar metabolism rather than starch mobilization.

PAW seed treatments induce SOD- and CAT-related antioxidant defense in osmotic stress-exposed pea

To explore the possible long-term antioxidant effects of PAW seed treatments, the activities of SOD, POD and CAT as representative enzymatic antioxidants were determined in the leaves of pea (Fig. 9). In plants grown under non-stressed conditions, all seed treatments increased the

activity of SOD (Fig. 9A). The trends in changes of POD and CAT activities were similar to those of SOD, but without statistically significant differences in pairwise comparisons (Fig. 9BC). These indicate a priming effect, likely mediated by mild ROS signalling or Zn cofactor activation, which may enhance the plant's antioxidant capacity to cope with subsequent environmental stresses. Under osmotic stress, SOD activity was significantly enhanced whereas CAT activity showed a non-significant decrease according to Tukey test, suggesting a stress-induced adjustment of antioxidant enzyme responses in DW plants. The activity of SOD was significantly further increased by PAW and was not modified by PA(W+Zn) or Zn treatments in osmotic stressed pea (Fig. 9A) indicating a strong PAW-specific SOD enzyme response. Moreover, CAT was significantly activated by PAW and PA(W+Zn), but not by Zn seed treatment in osmotically-stressed plant (Fig. 9C). POD activity was slightly (non-significantly according to Tukey test) increased by PAW and PA(W+Zn) seed treatments compared to the osmotic stress-exposed DW plants (Fig. 9B). According to two-way ANOVA, SOD activity showed significant treatment × PEG interaction ($p = 1.53 \times 10^{-6}$, Fig. 9A) and POD activity was significantly influenced by both treatment (p=0.01124) and PEG stress (p=0.02501), although post hoc comparisons revealed only moderate differences among individual treatment groups (Fig. 9B). Similarly, CAT activity exhibited a significant treatment × PEG interaction (p=0.03447), indicating that the effects of seed treatments depended on osmotic stress conditions. Under PEG stress, PAW and PA(W+Zn) treatments were associated with elevated CAT activity compared to PEG-treated DW plants (Fig. 9C). These findings are consistent with previous reports showing that various PAW application methods, including seed treatment combined with irrigation or irrigation alone, can induce antioxidant enzyme activity or gene expression, total antioxidant capacity, ascorbate and glutathione contents in different plant species (Adhikari et al., 2019; Bussmann et al., 2023; Ongrak et al., 2025; Zaboli et al., 2025, Ali and Dong, 2026). Under drought or PEG-triggered osmotic stress, the activated ABA signalling acts as a central regulator of antioxidant defense activation, coordinating the induction of key ROS-scavenging enzymes (e.g., Jiang and Zhang, 2001, 2002, 2004; Sheuli et al., 2025). This regulatory relationship may also operate in our system, as suggested by the further enhancement of osmotic stress-induced ABA signalling and the activation of antioxidant enzymes following PAW treatment. A possible additional ABA–ROS regulatory layer may involve PAW-induced enhancement of antioxidant capacity, which could modulate ABA-dependent ROS signalling in guard cells, thereby uncoupling increased ABA accumulation from further stomatal closure (see Fig. 6A,E).

PAW seed treatments upregulate ABA- and CK-associated genes in the leaf of osmotic stressed pea

The molecular mechanisms of PAW formulations-triggered responses to osmotic stress were examined by evaluating the expressions of ABA-dependent (*DEHIDRIN2, PsDHN2*) and –independent (*EARLY RESPONSIVE TO DEHYDRATION 1, PsERD1*) marker genes (Fig. 10). *PsDHN2*, encoding a group II LEA protein, was strongly induced by osmotic stress in both roots and leaves (Sahu et al., 2018), with a particularly high (~500-fold) response in leaves. The PA(W+Zn) seed treatment further amplified this induction (~700-fold), suggesting that the treatment primes the plant for enhanced LEA-mediated protective mechanisms, potentially contributing to improved cellular stabilization and osmotic stress tolerance (Fig. 10 AC). The Zn seed treatment resulted in decreased expression of *PsDHN2* compared to the DW seed treatment in the leaf of osmotic stress-exposed plants. Also, PAW seed treatment resulted in lower expression rate compared to DW (Fig. 10AC), which may reflect PAW-induced partial stress mitigation or a shift toward alternative protective mechanisms (e.g. antioxidant defence) in pea leaves. In the root of DW seed treated plants, the osmotic stress-triggered *PsDHN2* induction was more moderate (~40-fold, Fig. 10 BD), compared to the leaf. Seed treatments with either PAW, PA(W+Zn) or Zn further increased the expression of *PsDHN2* with PAW causing the highest induction (~430-fold, Fig. 10 BD). The more moderate stress-induced *PsDHN2* expression in roots compared to leaves suggests tissue-specific stress sensitivity, while the strong induction by PAW indicates that the treatment effectively primes root tissues for enhanced LEA-mediated protection.

In the leaf of DW plants, osmotic stress induced the expression of the *PsERD1* gene encoding a chloroplast-localized protease regulatory subunit, that responds to dehydration and high salinity before the accumulation of ABA (Nakashima et al., 1997). PA(W+Zn) and Zn further increased the expression (Fig. 10A) suggesting that these treatments potentiate protective mechanisms associated with chloroplast protein quality control under osmotic stress conditions. In the root, the PAW seed treatment slightly increased, while PA(W+Zn) and Zn decreased the expression of *PsERD1* (Fig. 10B) highlighting organ-specific stress responses. This reduction may indicate an alleviation of stress perception or the activation of alternative protective pathways in root tissues.

The expression of the proline synthesis gene, *Δ¹-PYRROLINE-5-CARBOXYLATE SYNTHETASE (PsP5CS)* exhibited coordinated yet treatment- and tissue-specific responses under osmotic stress (Fig. 10). In leaves, osmotic stress induced a slight upregulation of

PsP5CS, which was further enhanced by the PAW and Zn seed treatments, indicating stimulation of proline biosynthesis pathways. Consistent with this, proline content was significantly increased by the Zn treatment, while both PAW and PAW+Zn caused only non-significant increases (Fig. 6F), indicating that Zn enhances proline accumulation more efficiently. In roots, however, *PsP5CS* expression was downregulated by osmotic stress, with PAW and PA(W+Zn) treatments mitigating this suppression, while Zn further enhancing it, highlighting a contrasting regulatory pattern compared to leaves.

In recent years, CKs have emerged as key regulators of plant adaptation to osmotic stress. Elevated CK levels under such conditions can antagonize ABA signaling and its associated responses, delay leaf senescence, mitigate ROS-induced damage and lipid peroxidation, and ultimately promote plant growth and enhance tolerance to osmotic stress (Gujjar and Supaibulwatana, 2019). Furthermore, the PAW-associated decrease in leaf thickness in osmotically stressed pea may be due to limitations of cell divisions. Therefore, CK-related genes as molecular targets of PAW-effect were examined in the leaf, and also in the root system of pea. PAW and Zn seed treatments induced complex, tissue-specific changes in the expression of CK-related genes under both normal and osmotic stress conditions. The expression of *ARABIDOPSIS HISTIDINE KINASE* (*AHK*)-type CK receptor pea genes (*PsHK3, PsHK4*) were slightly downregulated by the PAW seed treatment under normal osmotic conditions. Osmotic stress upregulated *PsHK4*, and the PAW or Zn-associated treatments did not influence this pattern, while *PsHK3* expression did not show notable changes induced either by osmotic stress or seed treatments (Fig. 10A). The expressions of the pea homologs of *TYPE-A RESPONSE REGULATOR, PsRR5* and *PsRR17* were downregulated by PAW, while PA(W+Zn) and Zn seed treatments led to increased expression of these genes in non-stressed plants. The expression of both genes were induced by osmotic stress in DW plant, while PA(W+Zn) seed treatment resulted in further induction (Fig. 10A). The enhanced expression of response regulators under osmotic stress, particularly in case of PA(W+Zn) seed treatment, suggests an active feedback regulation of CK signaling pathways. These differential responses likely contribute to the observed reduction in leaf thickness (Fig. 5). In contrast, *PsRR9* expression was increased by the PAW and PA(W+Zn) seed treatments, and lowered by osmotic stress. The osmotic stress-induced downregulation of *PsRR9* was moderated by PAW and Zn seed treatments (Fig. 10A). In the root, *PsHK3*, *PsHK4* and also *PsRR5*, *PsRR9*, *PsRR17* were mainly downregulated by the seed treatments under normal osmotic conditions. Additionally, osmotic stress downregulated these genes, while PAW, PA(W+Zn) and Zn seed treatments

resulted in slight modifications in gene expressions (Fig. 10B). The relative transcript levels of *PsERD1, PsP5CS, PsHK3, PsHK4, PsRR5, PsRR9, PsRR17* in the leaf and root are shown in Fig. S4 and S5, respectively.

3. Conclusion

This study examined the effects of nitrate-dominant PAW and Zn-supplemented PAW, containing H_2O_2, and similar amounts of nitrate and nitrite, as seed priming agents on osmotic stress responses in pea.

Taken together, our results demonstrate that PAW and PA(W+Zn) seed treatments promote hilum opening, seed coat NO accumulation and improve seed nutrient composition. Importantly, PAW-induced priming activates ABA-SOD/CAT pathway, and is independent of proline osmotic regulation. To our knowledge, this is the first study to link PAW-induced osmotic stress tolerance to ABA signalling, and to identify *PsDHN2* as a robust marker of PAW-dependent osmotic stress responses. Moreover, leaf morphology, selected ion translocation and cytokinin signaling emerge as further targets underlying effects of PAW seed treatments under osmotic stress in pea. While PAW contains reactive species (e.g., H_2O_2, NO_3^- and NO_2^-) and has an acidic pH, the present study was designed to evaluate the integrated biological effect of PAW-based seed priming rather than to resolve the contribution of individual chemical components. Therefore, the specific roles of these constituents remain to be elucidated in future studies using targeted chemical controls.

Acknowledgements: This research was funded by the ‘Lendület’ MOMENTUM program of the Hungarian Academy of Sciences (LENDULET_2023-40). The study was also supported by the National Research, Development and Innovation Office (K146733 to GG). The XRF imaging facility was granted by the European Structural and Investment Funds (VEKOP-2.3.3-15-2016-00008). ÁS was supported by the János Bolyai Scholarship of the Hungarian Academy of Sciences under grant numbers BO-00113-23-8. Authors thank to László Bencs (HUN-REN Wigner RCP) for HR-CS-FAAS measurements. Authors are grateful to Éva Kapásné Török for her valuable help during the experiments.

Figure legends

Figure 1. Representative scanning electron microscopic (SEM) images showing the hilum region of pea seeds treated with distilled water (DW), PAW, PA(W+Zn) and Zn for 24 hours. (A) 40x magnification showing the whole hilum region. (B) 150× magnification of the hilum, micropyle-oriented side. (C) 150× magnification of hilum, opposite to micropyle-oriented side. Possible surface damages are indicated by white arrows.

Figure 2. (A) Values of NO levels (based on pixel intensity of DAF-FM probe) in seed coat sections from pea seeds treated with distilled water (DW), PAW, PA(W+Zn) and Zn for 24 hours. (B) Values of Zn levels (based on pixel intensity of Zinquin probe). Different letters indicate statistically significant differences as determined by Tukey's test ($p < 0.05$). Representative microscopic images of DAF-FM DA- (C) or Zinquin (D)-labelled seed coat sections. Scales= 200 µm (C) or 500 µm (D). Mean ± SE from 2 independent experiments (n = 10 seeds total; 3 sections per seed with 2 regions of interest measured per section).

Figure 3. (A) Representative XRF elemental maps of macro- and microelements in seeds treated with distilled water (DW), PAW, PA(W+Zn) and Zn for 24 hours. (B) Normalized values of elemental levels measured in seeds. Different letters indicate statistically significant differences as determined by Tukey's test ($p < 0.05$).

Figure 4. Primary root length (A, cm), lateral root length (B, cm), lateral root number (C, pcs), shoot length (D, cm) and leaf area (E, cm^2) of hydroponically-grown 3-weeks-old pea plants developed from seeds treated with distilled water (DW), PAW, PA(W+Zn) and Zn for 24 hours. Plants were grown hydroponically without or with PEG8000 (20 w/v%, 3days). Different letters indicate statistically significant differences as determined by Tukey's test ($p < 0.05$). (F) Representative photographs showing the effects of seed treatments on the size of pea leaves. Scale = 2 cm. Mean ± SE from 3 independent experiments (n = 9 biological units; 3 vessels per treatment per run). Primary root, shoot length and lateral root number reflect the mean of 36 plants; lateral root length reflects 10 roots/plant and leaf area represents 2 leaves/plant from the same insertion level.

Figure 5. (A) Thickness (µm) of tissue layers in the leaf of 3-weeks-old pea plants developed from seeds treated with distilled water (DW), PAW, PA(W+Zn) and Zn for 24 hours. Plants were grown hydroponically without or with PEG8000 (20 w/v%, 3days). Different letters indicate statistically significant differences as determined by Tukey's test ($p < 0.05$). (B) Representative microscopic images showing leaf tissue structure of pea in the presence or absence of PEG8000. Scale=200 µm. Mean ± SE from 2 independent experiments (n = 9 biological units; 3 vessels per treatment per run). Anatomical parameters reflect the mean of 36 plants (2 leaves/plant from the same insertion level).

Figure 6. Stomatal conductance (mmol m^{-2} s^{-1}, A), leaf relative water content (%, B), adaxial stomatal density (pcs/mm^2, C), abaxial stomatal density (pcs/mm^2, D), abscisic acid content in the leaf (µg/g fresh weight, E), proline content in the leaf (µmol/g fresh weight, F) of 3-weeks-old pea plants developed from seeds treated with distilled water (DW), PAW, PA(W+Zn) and Zn for 24 hours. Plants were grown hydroponically without or with PEG8000 (20 w/v%, 3 days). Different letters indicate statistically significant differences as determined by Tukey's test ($p < 0.05$). Mean ± SE from independent experiments. For g_s and RWC, n = 9 biological units (3 vessels/treatment across 3 runs); for stomatal density, n = 6 biological units (3 vessels/treatment across 2 runs, 3 images/plant); while ABA and proline reflect n = 6 biological replicates (2 runs, 3 technical replicates/sample).

Figure 7. Content of chlorophyll (mg/g fresh weight, A), carotenoid (mg/g fresh weight, B), anthocyanin (mg/g fresh weight, C), and values of F_v/F_m in leaves of pea plants grown from seeds treated with distilled water (DW), PAW, PA(W+Zn) and Zn for 24 hours. Plants were grown hydroponically without or with PEG8000 (20 w/v%, 3 days). Different letters indicate statistically significant differences as determined by Tukey's test ($p < 0.05$). Mean ± SE from 3 independent experiments (n = 9 biological units; 3 vessels per treatment per run). Photosynthetic pigments (A–C) were measured from each biological unit; Fv/Fm values reflect the mean of 36 plants total

Figure 8. Glucose content (mg/g fresh weight, A), sucrose content (mg/g fresh weight, B), starch content (mg/g fresh weight, C) in the leaf of pea plants developed from seeds treated with distilled water (DW), PAW, PA(W+Zn) or Zn for 24 hours. Plants were grown hydroponically without or with PEG8000 (20 w/v%, 3 days). Different letters indicate statistically significant differences as determined by Tukey's test ($p < 0.05$). Mean ± SE from 2 independent experiments (n = 6 biological units; 3 vessels per treatment per run). Each sample was measured in 3 technical replicates.

Figure 9. Activity of superoxide dismutase (unit/mg protein, A), peroxidase (unit/mg protein, B), catalase activity (unit/mg protein, C) in the leaf of 3-weeks-old pea developed from seeds treated with distilled water (DW), PAW, PA(W+Zn) and Zn for 24 hours. Plants were grown hydroponically without or with PEG8000 (20 w/v%, 3 days). Different letters indicate statistically significant differences as determined by Tukey's test ($p < 0.05$). Mean ± SE from 2 independent experiments (n = 6 biological units; 3 vessels per treatment per run). Each sample was measured in 3 technical replicates.

Figure 10. Heat maps representing the expression levels of the examined genes in the leaf (A) and root (B) of pea plants developed from seeds treated with distilled water (DW), PAW, PA(W+Zn) and Zn for 24 hours. Plants were grown hydroponically without or with PEG8000 (20 w/v%, 3 days). Relative transcript level of *PsDHN2* in leaf (C) and root (D). Data were normalized using the *P. sativum PP2A* gene as internal control. The relative transcript level in control samples was arbitrarily considered to be 1 for each gene.

Table 1. Characteristics of the prepared plasma-activated waters

Table 2. Evolution of plasma-activated waters during the 24 h period of priming at room temperature.

Table 3. Concentrations (ppm) of Zn, Fe, B, Mn, Cu, Ni is the leaf (A) and root (B) of 3-weeks-old pea plants developed from seeds treated with distilled water (DW), PA(W+Zn) and Zn for 24 hours. Plants were grown hydroponically without or with PEG8000 (20 w/v%, 3days). ppm = parts per million, RSD% = Relative Standard Deviation percentage, TF = Translocation factor.

Supplementary material:

Figure S1. Image of the surfatron generated surface-wave microwave discharge, with the plasma plume being in contact with the water to be treated.

Figure S2. Hilum pore diameter on the surface of pea seeds treated with distilled water (DW), PAW, PA(W+Zn) and Zn for 24 hours. Different letters indicate statistically significant differences as determined by Tukey's test ($p < 0.05$). Mean ± SE (n = 6 individual seeds per

treatment). On each seed, five distinct locations along the hilum fissure were measured to determine the mean value for that individual.

Figure S3. Representative photographs taken from 3-weeks-old pea plants grown from seeds treated with distilled water (DW), PAW, PA(W+Zn) and Zn for 24 hours. Plants were grown hydroponically without or with PEG8000 (20 w/v%, 3 days). Scale=10 cm.

Figure S4. Relative transcript level of osmotic stress- and CK-related genes in leaf of pea plants developed from seeds treated with distilled water (DW), PAW, PA(W+Zn) and Zn for 24 hours. Plants were grown hydroponically without or with PEG8000 (20 w/v%, 3 days). Data were normalized using the *P. sativum PP2A* gene as internal control. The relative transcript level in control samples was arbitrarily considered to be 1 for each gene.

Figure S5. Relative transcript level of osmotic stress- and CK-related genes in root of pea plants developed from seeds treated with distilled water (DW), PAW, PA(W+Zn) and Zn for 24 hours. Plants were grown hydroponically without or with PEG8000 (20 w/v%, 3 days). Data were normalized using the *P. sativum PP2A* gene as internal control. The relative transcript level in control samples was arbitrarily considered to be 1 for each gene.

Table S1. Primers used for this study.

Table S2. F and p values from two-way ANOVA evaluating the effects of seed treatment and PEG-induced osmotic stress on the quantified physiological and biochemical parameters.

Table S3. Element content values and translocation factor values based on dry weight of whole shoot or root. Data are shown as mean ± SE.

References

Adhikari, B., Adhikari, M., Ghimire, B., Park, G., Choi, E.H., 2019. Cold Atmospheric Plasma-Activated Water Irrigation Induces Defense Hormone and Gene expression in Tomato seedlings. Sci. Rep. 9, 16080. https://doi.org/10.1038/s41598-019-52646-z

Barroso, J.B., Corpas, F.J., Carreras, A., Rodríguez-Serrano, M., Esteban, F.J., Fernández-Ocaña, A., Chaki, M., Romero-Puertas, M.C., Valderrama, R., Sandalio, L.M., Del Río, L.A., 2006. Localization of S-nitrosoglutathione and expression of S-nitrosoglutathione reductase in pea plants under cadmium stress. J. Exp. Bot. 57, 1785–1793. https://doi.org/10.1093/jxb/erj175

Bates, L.S., Waldren, R.P., Teare, I.D., 1973. Rapid determination of free proline for water-stress studies. Plant and Soil 1973 39, 205–207. https://doi.org/10.1007/BF00018060

Billah, M., Sajib, S.A., Roy, N.C., Rashid, M.M., Reza, M.A., Hasan, M.M., Talukder, M.R., 2020. Effects of DBD air plasma treatment on the enhancement of black gram (Vigna mungo l.) seed germination and growth. Arch. Biochem. Biophys. 681, 108253. https://doi.org/10.1016/j.abb.2020.108253

Biswas, A., Sarkar, S., Das, S., Dutta, S., Roy Choudhury, M., Giri, A., Bera, B., Bag, K., Mukherjee, B., Banerjee, K., Gupta, D., Paul, D., Choudhury, R.M., 2025. Water scarcity: A global hindrance to sustainable development and agricultural production – A critical review of the impacts and adaptation strategies, in: Cambridge Prisms: Water. Cambridge University Press. https://doi.org/10.1017/wat.2024.16

Bodor, T., Fejes, G., Chaumont, N., Bailly, C., Solti, Á., Gracheva, M., Szenti, I., Kónya, Z., Rónavári, A., Kutasi, K., Kolbert, Zs., 2026. Effect of seed priming by zinc-ion and zinc-oxide nanoparticle enriched plasma-activated water in osmotic-stressed Arabidopsis thaliana. Plasma Processes and Polymers, in press

Bussmann, F., Krüger, A., Scholz, C., Brust, H., Stöhr, C., 2023. Long-Term Effects of Cold Atmospheric Plasma-Treated Water on the Antioxidative System of Hordeum vulgare. Journal of Plant Growth Regulation 42, 3274–3290. https://doi.org/10.1007/S00344-022-10789-W

Chamizo-Ampudia, A., Sanz-Luque, E., Llamas, A., Galvan, A., Fernandez, E., 2017. Nitrate Reductase Regulates Plant Nitric Oxide Homeostasis. Trends Plant Sci. 22, 163–174. https://doi.org/10.1016/j.tplants.2016.12.001

Cheng, H., Chen, X., Fang, J., An, Z., Hu, Y., Huang, H., 2018. Comparative transcriptome analysis reveals an early gene expression profile that contributes to cold resistance in Hevea brasiliensis (the Para rubber tree). Tree Physiol. 38, 1409–1423. https://doi.org/10.1093/treephys/tpy014

da Silva, E.C., Nogueira, R.J.M.C., da Silva, M.A., de Albuquerque, M.B., 2011. p Stress and Plant Nutrition. Plant Stress 5, 32–41.

Dahal, R., Dhakal, O.B., Acharya, T.R., Lamichhane, P., Gautam, S., Chalise, R., Kaushik, N., Choi, E.H., Kaushik, N.K., 2024. Investigating plasma activated water as a sustainable treatment for improving growth and nutrient uptake in maize and pea plant. Plant Physiology and Biochemistry 216, 109203. https://doi.org/10.1016/j.plaphy.2024.109203

Dhindsa, R.S., Plumb-dhindsa, P., Thorpe, T.A., 1981. Leaf senescence: Correlated with increased levels of membrane permeability and lipid peroxidation, and decreased levels of superoxide dismutase and catalase. J. Exp. Bot. 32, 93–101. https://doi.org/10.1093/jxb/32.1.93

Eid, E.M., Shaltout, K.H., 2016. Bioaccumulation and translocation of heavy metals by nine native plant species grown at a sewage sludge dump site. Int. J. Phytoremediation 18, 1075–1085. https://doi.org/10.1080/15226514.2016.1183578

Gohari, G., Spanos, A., Ioannou, A., Efstathiou, I., Panahirad, S., Kolbert, Z., Fotopoulos, V., 2026. Seed priming approaches for climate-resilient agriculture. J. Exp. Bot. 77, 2013–2026. https://doi.org/10.1093/jxb/eraf440

Gone, S.S.J.C., Singh, R.K., 2025. Enhancing Pea Seed Sprouting and Quality with Plasma-Activated Water. Food Bioproc. Tech. 18, 9546–9560. https://doi.org/10.1007/s11947-025-03993-5

González-Bernáldez, F., López-Sáez, J.F., García-Ferrero, G., 1968. Effect of osmotic pressure on root growth, cell cycle and cell elongation. Protoplasma 65, 255–262. https://doi.org/10.1007/BF01682531

Gujjar, R.S., Supaibulwatana, K., 2019. The Mode of Cytokinin Functions Assisting Plant Adaptations to Osmotic Stresses. Plants 8, 542. https://doi.org/10.3390/plants8120542

Ha, S., Vankova, R., Yamaguchi-Shinozaki, K., Shinozaki, K., Tran, L.S.P., 2012. Cytokinins: Metabolism and function in plant adaptation to environmental stresses. Trends Plant Sci. 17, 172–179. https://doi.org/10.1016/j.tplants.2011.12.005

Hansen, J., Møller, I., 1975. Percolation of starch and soluble carbohydrates from plant tissue for quantitative determination with anthrone. Anal. Biochem. 68, 87–94. https://doi.org/10.1016/0003-2697(75)90682-X

Helmersson, A., Von Arnold, S., Bozhkov, P. V., 2008. The Level of Free Intracellular Zinc Mediates Programmed Cell Death/Cell Survival Decisions in Plant Embryos. Plant Physiol. 147, 1158–1167. https://doi.org/10.1104/pp.108.122598

Horváth, E., Csiszár, J., Gallé, Á., Poór, P., Szepesi, Á., Tari, I., 2015. Hardening with salicylic acid induces concentration-dependent changes in abscisic acid biosynthesis of tomato under salt stress. J. Plant Physiol. 183, 54–63. https://doi.org/10.1016/j.jplph.2015.05.010

Janda, M., Stancampiano, A., di Natale, F., Machala, Z., 2025. Short Review on Plasma–Aerosol Interactions. Plasma Proc. Polym. 22, 2400275. https://doi.org/10.1002/ppap.202400275

Jiang, M., Zhang, J., 2002. Water stress-induced abscisic acid accumulation triggers the increased generation of reactive oxygen species and up-regulates the activities of antioxidant enzymes in maize leaves. J. Exp. Bot. 53, 2401–2410. https://doi.org/10.1093/JXB/ERF090

Jiang, M., Zhang, J., 2001. Effect of Abscisic Acid on Active Oxygen Species, Antioxidative Defence System and Oxidative Damage in Leaves of Maize Seedlings. Plant Cell Physiol. 42, 1265–1273. https://doi.org/10.1093/PCP/PCE162

Jiang, M., Zhang, J., 2004. Abscisic Acid and Antioxidant Defense in Plant Cells. Acta Bot. Sin. 46, 1–9.

Kalinowska, M., Sienkiewicz-Gromiuk, J., Świderski, G., Pietryczuk, A., Cudowski, A., Lewandowski, W., 2020. Zn(II) Complex of Plant Phenolic Chlorogenic Acid: Antioxidant, Antimicrobial and Structural Studies. Materials 13, 3745. https://doi.org/10.3390/MA13173745

Khotimchenko, M.Y., Kolenchenko, E.A., Khotimchenko, Y.S., 2008. Zinc-binding activity of different pectin compounds in aqueous solutions. J. Colloid Interface Sci. 323, 216–222. https://doi.org/10.1016/j.jcis.2008.04.013

Kolbert, Z., Petô, A., Lehotai, N., Feigl, G., Ördög, A., Erdei, L., 2012. In vivo and in vitro studies on fluorophore-specificity. Acta Biologica Szegediensis, 56(1), pp. 37–41.

Kukri, A., Czékus, Z., Gallé, Á., Nagy, G., Zsindely, N., Bodai, L., Galgóczy, L., Hamow, K.Á., Szalai, G., Ördög, A., Poór, P., 2024. Exploring the effects of red light night break on the defence mechanisms of tomato against fungal pathogen Botrytis cinerea. Physiol. Plant. 176. https://doi.org/10.1111/ppl.14504

Kutasi, K., Bencs, L., Tóth, Z., Milošević, S., 2023. The role of metals in the deposition of long-lived reactive oxygen and nitrogen species into the plasma-activated liquids. Plasma Processes and Polymers 20. https://doi.org/10.1002/ppap.202200143

Kutasi, K., Nöel, C., Belmonte, T., Hartmann, P., 2026. Low-power atmospheric-pressure surface-wave microwave discharge in contact with batch and flowing liquids. J. Phys. D Appl. Phys. 59, 015208. https://doi.org/10.1088/1361-6463/ae2aee

Kutasi, K., Popović, D., Krstulović, N., Milošević, S., 2019. Tuning the composition of plasma-activated water by a surface-wave microwave discharge and a kHz plasma jet. Plasma Sources Sci. Technol. 28, 095010. https://doi.org/10.1088/1361-6595/ab3c2f

Lecoeur, J., Wery, J., Turc, O., Tardieu, F., 1995. Expansion of pea leaves subjected to short water deficit: cell number and cell size are sensitive to stress at different periods of leaf development. J. Exp. Bot. 46, 1093–1101. https://doi.org/10.1093/jxb/46.9.1093

Li, L., Zhang, L., Dong, Y., 2025. Seed priming with cold plasma mitigated the negative influence of drought stress on growth and yield of rapeseed (Brassica napus L.). Ind. Crops Prod. 228, 120899. https://doi.org/10.1016/j.indcrop.2025.120899

Liao, Z., Boubakri, H., Chen, B., Farooq, M., Lai, Z., Kou, H., Fan, J., 2025. Biofertilizers as an eco-friendly approach to combat drought stress in plants. Biocatal. Agric. Biotechnol. 64, 103510. https://doi.org/10.1016/j.bcab.2025.103510

Livak, K.J., Schmittgen, T.D., 2001. Analysis of Relative Gene Expression Data Using Real-Time Quantitative PCR and the 2−ΔΔCT Method. Methods 25, 402–408. https://doi.org/10.1006/meth.2001.1262

Lukes, P., Dolezalova, E., Sisrova, I., Clupek, M., 2014. Aqueous-phase chemistry and bactericidal effects from an air discharge plasma in contact with water: Evidence for the formation of peroxynitrite through a pseudo-second-order post-discharge reaction of H2O 2 and HNO2. Plasma Sources Sci. Technol. 23. https://doi.org/10.1088/0963-0252/23/1/015019

Luo, P., Shen, Y., Jin, S., Huang, S., Cheng, X., Wang, Z., Li, P., Zhao, J., Bao, M., Ning, G., 2016. Overexpression of Rosa rugosa anthocyanidin reductase enhances tobacco tolerance to abiotic stress through increased ROS scavenging and modulation of ABA signaling. Plant Science 245, 35–49. https://doi.org/10.1016/j.plantsci.2016.01.007

Magné, C., Larher, F., 1992. High sugar content of extracts interferes with colorimetric determination of amino acids and free proline. Anal. Biochem. 200, 115–118. https://doi.org/10.1016/0003-2697(92)90285-F

Marolt, G., Gričar, E., Pihlar, B., Kolar, M., 2020. Complex Formation of Phytic Acid With Selected Monovalent and Divalent Metals. Front. Chem. 8. https://doi.org/10.3389/fchem.2020.582746

Michel, B.E., Kaufmann, M.R., 1973. The Osmotic Potential of Polyethylene Glycol 6000. Plant Physiol. 51, 914. https://doi.org/10.1104/PP.51.5.914

Mohammadi Alagoz, S., Asgari Lajayer, B., Ghorbanpour, M., 2023. Proline and soluble carbohydrates biosynthesis and their roles in plants under abiotic stresses, in: Ghorbanpour, M., Shahid, M.A. (Eds.), Plant Stress Mitigators: Types, Techniques and Functions. Academic Press, pp. 169–185. https://doi.org/10.1016/B978-0-323-89871-3.00027-6

Mohn, M.A., Thaqi, B., Fischer-Schrader, K., 2019. Isoform-specific NO synthesis by arabidopsis thaliana nitrate reductase. Plants 8. https://doi.org/10.3390/plants8030067

Muhammad Aslam, M., Waseem, M., Jakada, B.H., Okal, E.J., Lei, Z., Saqib, H.S.A., Yuan, W., Xu, W., Zhang, Q., 2022. Mechanisms of Abscisic Acid-Mediated Drought Stress Responses in Plants. International Journal of Molecular Sciences 2022, Vol. 23, Page 1084 23, 1084. https://doi.org/10.3390/ijms23031084

Naik, P.K., Ruban, J.S., Naidu, S.A., Fetricia, J.P., 2022. Effect of Drought Stress and Mineral Nutrition in Plant Growth and Development. Int. J. Curr. Microbiol. Appl. Sci. 11, 109–114. https://doi.org/10.20546/ijcmas.2022.1105.014

Nakashima, K., Kiyosue, T., Yamaguchi-Shinozaki, K., Shinozaki, K., 1997. A nuclear gene, erd1, encoding a chloroplast-targeted Clp protease regulatory subunit homolog is not only induced by water stress but also developmentally up-regulated during senescence in Arabidopsis thaliana. Plant J. 12, 851–861. https://doi.org/10.1046/j.1365-313X.1997.12040851.x

Ongrak, P., Poolyarat, N., Harakotr, B., Jirakiattikul, Y., Rithichai, P., 2025. Plasma-Activated Water (PAW) Enhances Seed Germination and Improves Biochemical Quality in Kangkong (Ipomoea aquatica Forssk.) Microgreens. Horticulturae 2025, Vol. 11, Page 1218 11, 1218. https://doi.org/10.3390/horticulturae11101218

Peña, F. de la, Prestat, E., Fauske, V.T., Burdet, P., Lähnemann, J., Jokubauskas, P., Furnival, T., Nord, M., Ostasevicius, T., MacArthur, K.E., Johnstone, D.N., Sarahan, M., Taillon, J., Aarholt, T., pquinn-dls, Migunov, V., Eljarrat, A., Caron, J., Francis, C., Nemoto, T., Poon, T., Mazzucco, S., actions-user, Tappy, N., Cautaerts, N., Somnath, S., Slater, T., Walls, M., Winkler, F., Ånes, H.W., n.d. hyperspy/hyperspy: Release v1.7.2. https://doi.org/10.5281/ZENODO.7090040

Priatama, R.A., Beak, H.K., Park, S., Song, I., Park, S.J., Kim, S.B., Lee, Y.K., 2025. Tomato yield enhancement with plasma-activated water as an alternative nitrogen source. BMC Plant Biol. 25, 668. https://doi.org/10.1186/s12870-025-06701-9

Rathore, V., Tiwari, B.S., Nema, S.K., 2021. Treatment of Pea Seeds with Plasma Activated Water to Enhance Germination, Plant Growth, and Plant Composition. Plasma Chemistry and Plasma Processing 42, 109–129. https://doi.org/10.1007/s11090-021-10211-5

Rockel, P., Strube, F., Rockel, A., Wildt, J., Kaiser, W.M., 2002. Regulation of nitric oxide (NO) production by plant nitrate reductase in vivo and in vitro. J. Exp. Bot. 53, 103–110. https://doi.org/10.1093/jexbot/53.366.103

Saha, D., Choyal, P., Mishra, U.N., Dey, P., Bose, B., Prathibha, M.D., Gupta, N.K., Mehta, B.K., Kumar, P., Pandey, S., Chauhan, J., Singhal, R.K., 2022. Drought stress responses and inducing tolerance by seed priming approach in plants. Plant Stress 4, 100066. https://doi.org/10.1016/j.stress.2022.100066

Sahu, B., Sahu, A.K., Sahu, A., Naithani, S.C., 2018. Gene expression of late embryogenesis abundant proteins, small heat shock proteins and peroxiredoxin and oxidation of lipid and protein during loss and re-establishment of desiccation tolerance in Pisum sativum seeds. South African Journal of Botany 119, 28–36. https://doi.org/10.1016/j.sajb.2018.08.004

Sheuli, S.A., Arafin, M.S., Sultana, S., Rabbi, M.A., Ghosh, A., 2025. Exogenous salicylic acid, abscisic acid, and shikimic acid enhance drought tolerance in tea by modulating antioxidant defense and osmotic regulation. PLoS One 20, e0331456. https://doi.org/10.1371/JOURNAL.PONE.0331456

Sims, D.A., Gamon, J.A., 2002. Relationships between leaf pigment content and spectral reflectance across a wide range of species, leaf structures and developmental stages. Remote Sens. Environ. 81, 337–354. https://doi.org/10.1016/S0034-4257(02)00010-X

Song, F., Yang, Q., Huang, J., Guo, Z., Li, Y., Deng, W., 2026. Plant drought stress: physiological, biochemical and molecular mechanisms. Plant Stress 19, 101153. https://doi.org/10.1016/j.stress.2025.101153

Stanton, C., Sanders, D., Krämer, U., Podar, D., 2022. Zinc in plants: Integrating homeostasis and biofortification. Mol. Plant 15, 65–85. https://doi.org/10.1016/j.molp.2021.12.008

Stöhr, C., Strube, F., Marx, G., Ullrich, W.R., Rockel, P., 2001. A plasma membrane-bound enzyme of tobacco roots catalyses the formation of nitric oxide from nitrite. Planta 212, 835–841. https://doi.org/10.1007/s004250000447

Stoleru, V., Burlica, R., Mihalache, G., Dirlau, D., Padureanu, S., Teliban, G.C., Astanei, D., Cojocaru, A., Beniuga, O., Patras, A., 2020. Plant growth promotion effect of plasma activated water on Lactuca sativa L. cultivated in two different volumes of substrate. Sci. Rep. 10, 20920. https://doi.org/10.1038/s41598-020-77355-w

Tanaka, Y., Sano, T., Tamaoki, M., Nakajima, N., Kondo, N., Hasezawa, S., 2006. Cytokinin and auxin inhibit abscisic acid-induced stomatal closure by enhancing ethylene production in Arabidopsis. J. Exp. Bot. 57, 2259–2266. https://doi.org/10.1093/jxb/erj193

Tari, I., Csiszar, J., Horvath, E., Poor, P., Takacs, Z., Szepesi, A., 2015. The alleviation of the adverse effects of salt stress in the tomato plant by salicylic acid shows a timeand organ-specific antioxidant response. Acta Biol. Crac. Ser. Bot. 57, 21–30. https://doi.org/10.1515/abcsb-2015-0008

Thakur, M., Tiwari, S., Kataria, S., Anand, A., 2022. Recent advances in seed priming strategies for enhancing planting value of vegetable seeds. Sci. Hortic. 305, 111355. https://doi.org/10.1016/j.scienta.2022.111355

Than, H.A.Q., Pham, Thien Huu, Nguyen, D.K.V., Pham, Thuong Hoai, Khacef, A., 2021. Non-thermal Plasma Activated Water for Increasing Germination and Plant Growth of Lactuca sativa L. Plasma Chemistry and Plasma Processing 2021 42:1 42, 73–89. https://doi.org/10.1007/s11090-021-10210-6

Upadhyaya, A., Sankhla, D., Davis, T.D., Sankhla, N., Smith, B.N., 1985. Effect of Paclobutrazol on the Activities of some Enzymes of Activated Oxygen Metabolism and Lipid Peroxidation in Senescing Soybean Leaves. J. Plant Physiol. 121, 453–461. https://doi.org/10.1016/S0176-1617(85)80081-X

Upretee, P., Bandara, M.S., Tanino, K.K., 2024. The Role of Seed Characteristics on Water Uptake Preceding Germination. Seeds 2024, Vol. 3, Pages 559-574 3, 559–574. https://doi.org/10.3390/seeds3040038

Verslues, P.E., Agarwal, M., Katiyar-Agarwal, S., Zhu, J., Zhu, J.K., 2006. Methods and concepts in quantifying resistance to drought, salt and freezing, abiotic stresses that affect plant water status. Plant J. 45, 523–539. https://doi.org/10.1111/J.1365-313X.2005.02593.X

Wang, P., Du, Y., Li, Y., Ren, D., Song, C.P., 2010. Hydrogen peroxide-mediated activation of MAP kinase 6 modulates nitric oxide biosynthesis and signal transduction in Arabidopsis. Plant Cell 22, 2981–2998. https://doi.org/10.1105/tpc.109.072959

Wang, X., Hargrove, M.S., 2013. Nitric oxide in plants: the roles of ascorbate and hemoglobin. PLoS One 8. https://doi.org/10.1371/journal.pone.0082611

Yoshida, T., Mogami, J., Yamaguchi-Shinozaki, K., 2014. ABA-dependent and ABA-independent signaling in response to osmotic stress in plants. Curr. Opin. Plant Biol. 21, 133–139. https://doi.org/10.1016/j.pbi.2014.07.009

Zaboli, M., Nejad-Alimoradi, F., Rostami, F., keramat, B., Mousavi, E.A., Nasibi, F., 2025. Seed priming and irrigating with plasma-activated water improve the growth and drought resistance in Poa pratensis. BMC Plant Biol. 25, 1747. https://doi.org/10.1186/s12870-025-07742-w

Table 1. Concentration of species in the different plasma-activated waters

Sample	Ageing	$[H_2O_2]$ [mg L^{-1}]	$[NO_2^-]$ [mg L^{-1}]	$[NO_3^-]$ [mg L^{-1}]	$[Zn^{2+}]$ [mg L^{-1}]	pH
PAW	1 day	0	10±2	30±3	-	3.9±0.2
PAWZn	1 day	10±2	29±3	14±3	27.9±0.8	5.7±0.2
PA(W+Zn)	0 min	6±1	19±2	20±3	14±0.8	4.7±0.1
	2 h	3±1	13±2	25±2	14±0.8	4.7±0.1
	4 h	3±1	13±2	25±2	14±0.8	4.7±0.1
	24 h	0	5±2	30±2	14±0.8	5.1±0.1

Table 2. Concentrations (ppm) of Zn, Fe, B, Mn, Cu, Ni is the leaf (A) and root (B) of 3-weeks-old pea plants developed from seeds treated with distilled water (DW), PA(W+Zn) and Zn for 24 hours. Plants were grown hydroponically without or with PEG8000 (20 w/v%, 3days). ppm = parts per million, RSD% = Relative Standard Deviation percentage, TF = Translocation factor.

A Leaf		Zn			Fe			B		
		ppm	RSD%	TF	ppm	RSD%	TF	ppm	RSD%	TF
Without PEG	**DW**	54.01	4.25	1.04	266.33	2.39	1.28	15.94	8.18	1.90
	PAW	61.37	2.42	1.03	300.41	2.82	0.95	16.29	1.85	1.96
	PA(W+Zn)	80.47	1.86	1.28	259.00	2.88	0.79	13.70	5.72	2.21
	Zn	70.67	1.76	1.18	305.48	1.89	0.92	13.10	8.44	2.12
With PEG	**DW**	61.05	2.55	1.72	169.87	2.01	1.24	2.60	6.74	11.05
	PAW	61.37	2.81	3.07	239.17	2.64	2.22	3.44	6.81	7.44
	PA(W+Zn)	81.24	3.91	2.93	159.52	2.42	1.21	3.23	15.31	7.37
	Zn	76.19	4.36	3.65	219.49	1.60	1.73	2.30	6.09	11.48
Leaf		**Mn**			**Cu**			**Ni**		
		ppm	RSD%	TF	ppm	RSD%	TF	ppm	RSD%	TF
Without PEG	**DW**	78.78	0.92	0.67	11.80	2.15	1.21	0.33	7.29	1.69
	PAW	163.85	1.63	0.42	12.58	1.32	1.15	0.42	25.14	1.41
	PA(W+Zn)	123.29	1.26	0.45	12.86	1.32	1.12	0.51	20.44	1.04
	Zn	157.71	2.15	0.46	13.98	1.03	1.02	0.58	27.34	0.96
With PEG	**DW**	28.17	1.86	1.93	7.02	2.81	2.09	0.01	3.06	51.55
	PAW	27.30	1.99	2.23	6.45	3.52	2.31	0.12	21.27	53.50
	PA(W+Zn)	22.46	2.06	2.00	6.98	2.20	1.97	0.01	1.73	52.53
	Zn	22.58	1.41	2.78	6.47	2.48	2.14	0.01	46.76	52.00

B Root		Zn		Fe		B	
		ppm	RSD%	ppm	RSD%	ppm	RSD%
Without PEG	**DW**	51.92	1.52	208.46	4.41	15.94	8.18
	PAW	59.39	1.43	316.29	1.66	16.29	1.85
	PA(W+Zn)	62.64	1.91	326.79	0.85	13.70	5.72
	Zn	59.80	0.94	333.08	1.51	13.10	8.44
With PEG	**DW**	35.43	1.78	136.54	1.15	2.60	6.74
	PAW	20.02	2.46	107.65	1.33	3.44	6.81

	PA(W+Zn)	27.72	1.54	131.72	1.32	3.23	15.31
	Zn	20.89	2.08	126.51	1.13	2.30	6.09
Root		**Mn**		**Cu**		**Ni**	
		ppm	RSD%	ppm	RSD%	ppm	RSD%
Without PEG	**DW**	78.78	0.92	11.80	2.15	0.33	7.29
	PAW	163.85	1.63	12.58	1.32	0.42	25.14
	PA(W+Zn)	123.29	1.26	12.86	1.32	0.51	20.44
	Zn	157.71	2.15	13.98	1.03	0.58	27.34
With PEG	**DW**	28.17	1.86	7.02	2.81	0.01	3.06
	PAW	27.30	1.99	6.45	3.52	0.01	21.27
	PA(W+Zn)	22.46	2.06	6.98	2.20	0.01	1.73
	Zn	22.58	1.41	6.47	2.48	0.01	46.76

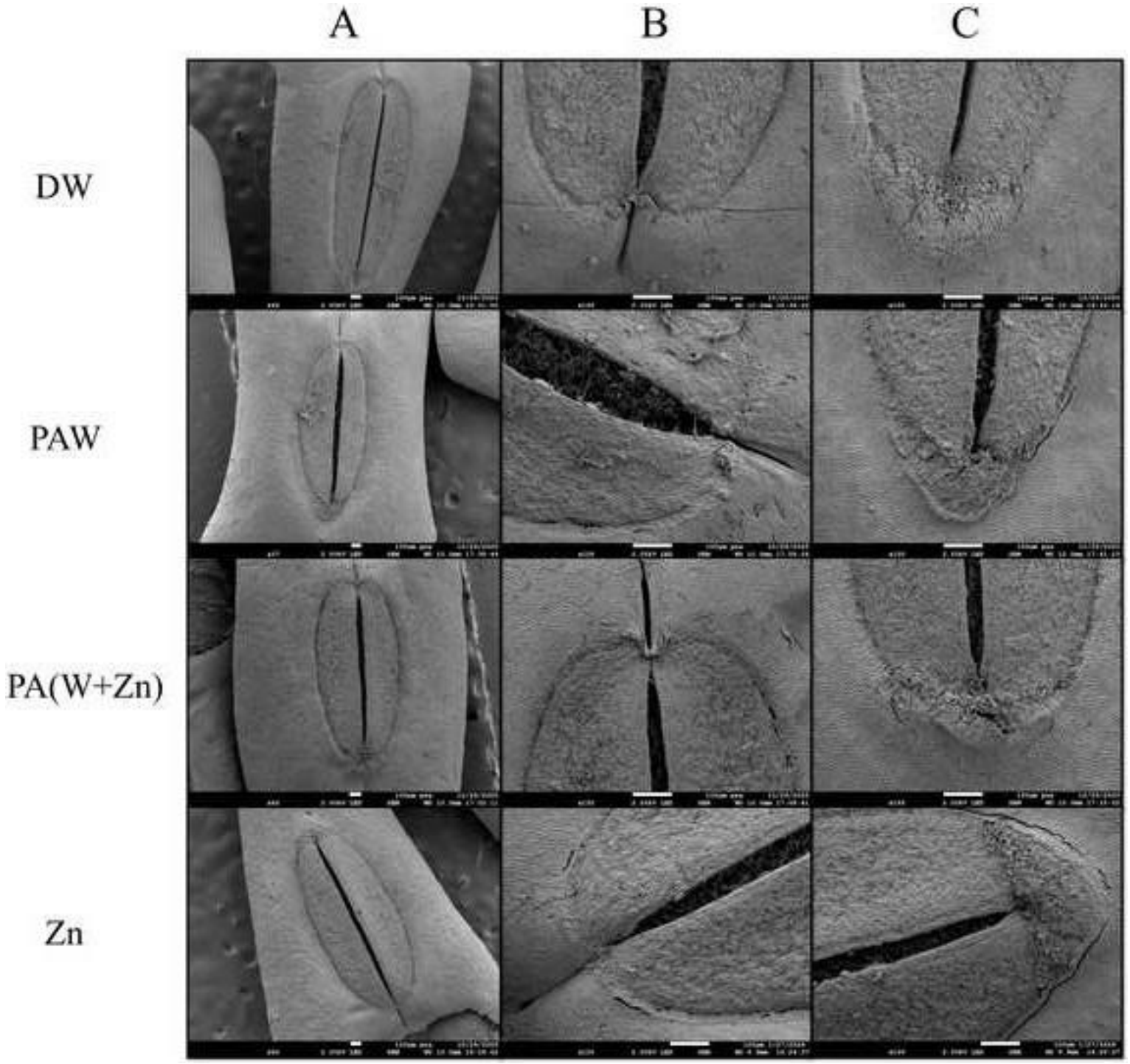
A
B
C
DW
PAW
PA(W+Zn)
Zn

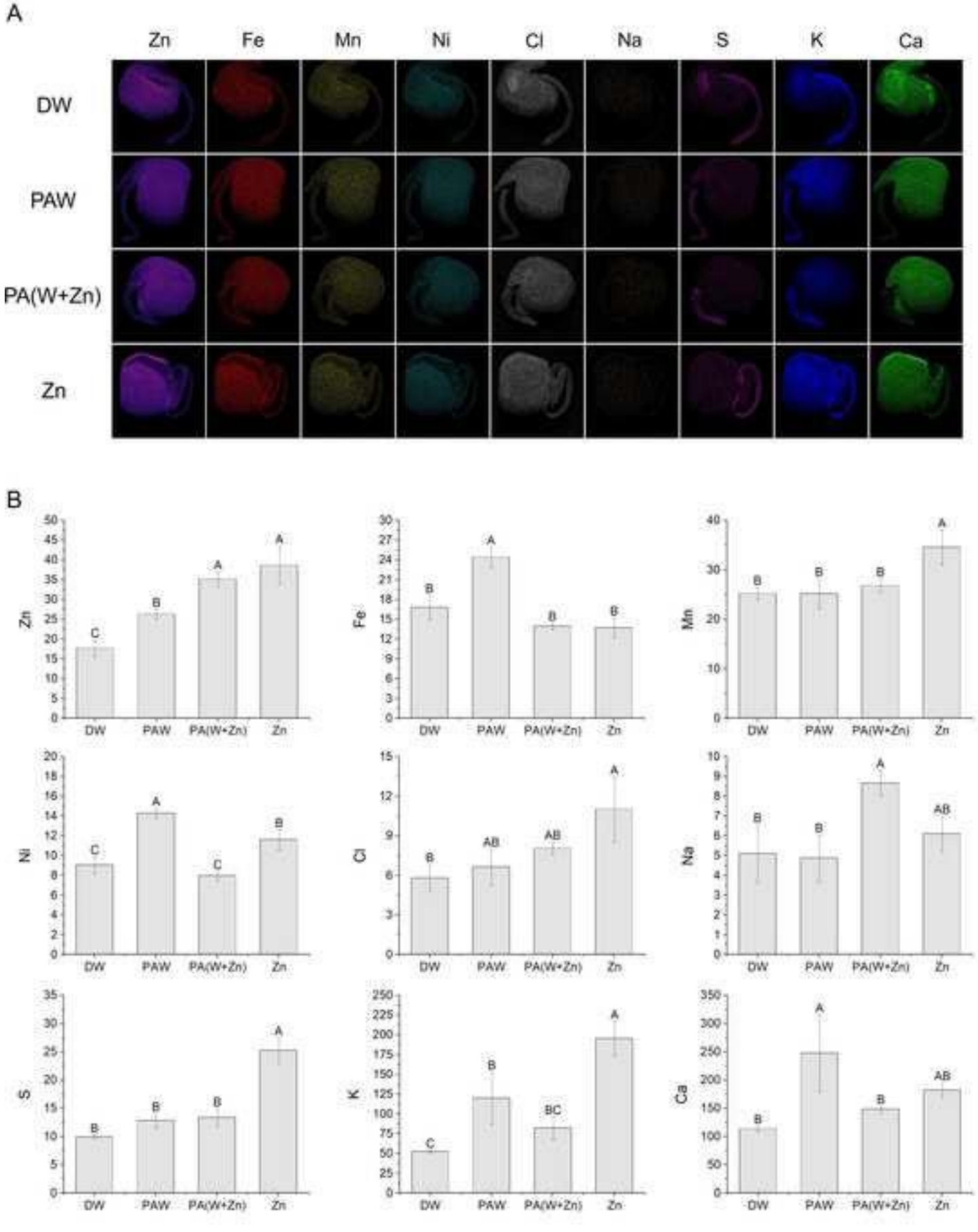
A
Zn
Fe
Mn
Ni
Cl
Na
S
K
Ca
DW
PAW
PA(W+Zn)
Zn
B
Zn
Fe
Mn
Ni
Cl
Na
S
K
Ca
DW
PAW
PA(W+Zn)
Zn

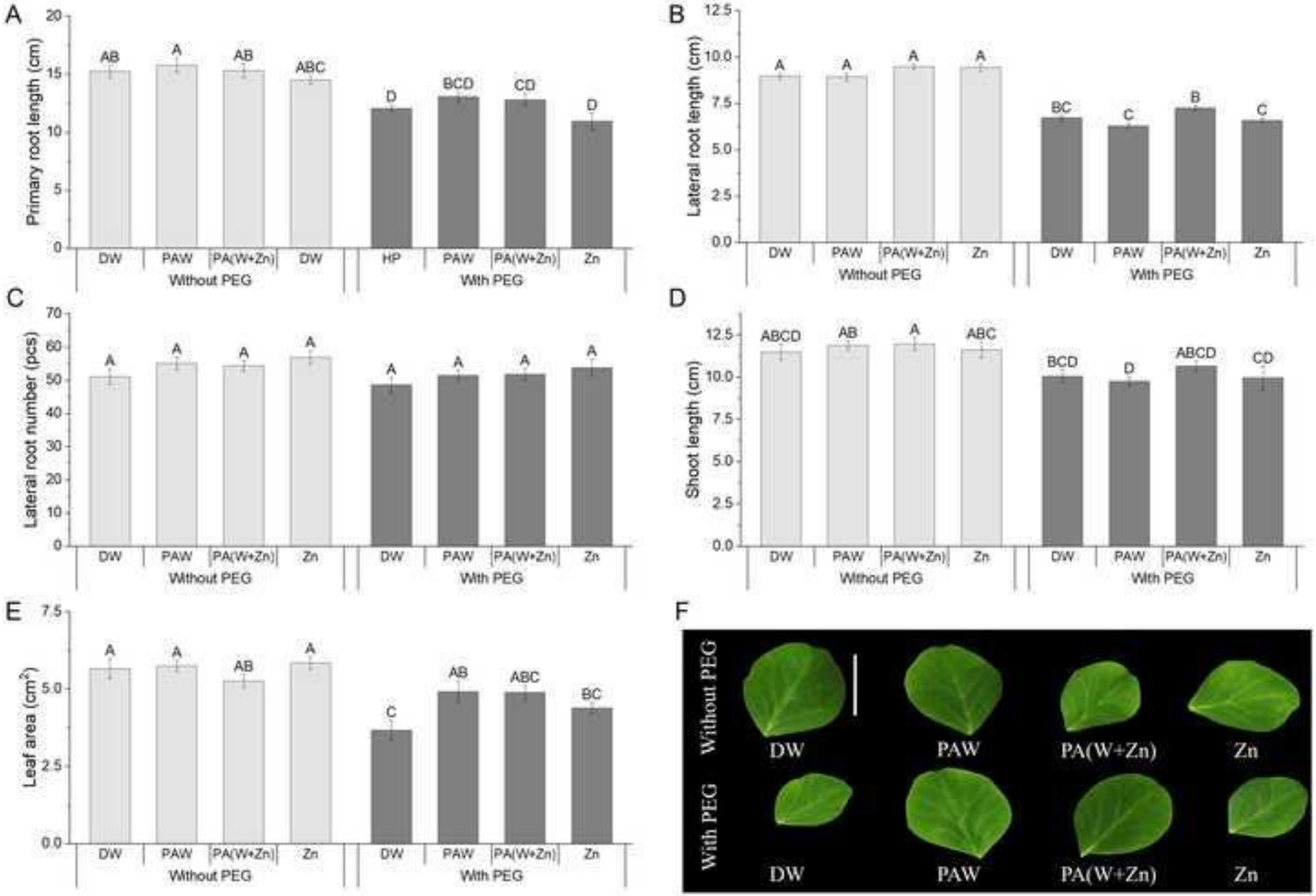
A
Primary root length (cm)
AB
A
AB
ABC
D
BCD
CD
D
DW
PAW
PA(W+Zn)
DW
HP
PAW
PA(W+Zn)
Zn
Without PEG
With PEG
B
Lateral root length (cm)
A
A
A
A
BC
C
B
C
C
Lateral root number (pcs)
D
Shoot length (cm)
ABCD
AB
A
ABC
BCD
D
ABCD
CD
E
Leaf area (cm²)
AB
ABC
BC
F
Without PEG
With PEG
DW
PAW
PA(W+Zn)
Zn

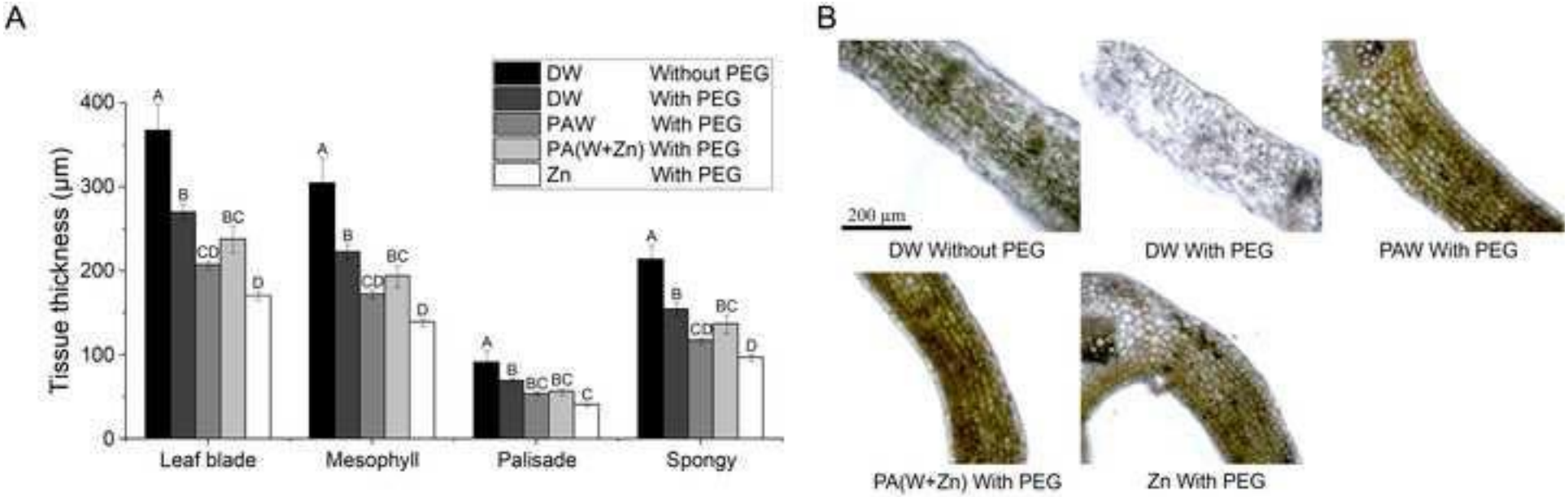
A
B
DW Without PEG
DW With PEG
PAW With PEG
PA(W+Zn) With PEG
Zn With PEG
Tissue thickness (µm)
400
300
200
100
0
Leaf blade
Mesophyll
Palisade
Spongy
A
B
CD
BC
D
C
200 µm
DW Without PEG
DW With PEG
PAW With PEG
PA(W+Zn) With PEG
Zn With PEG

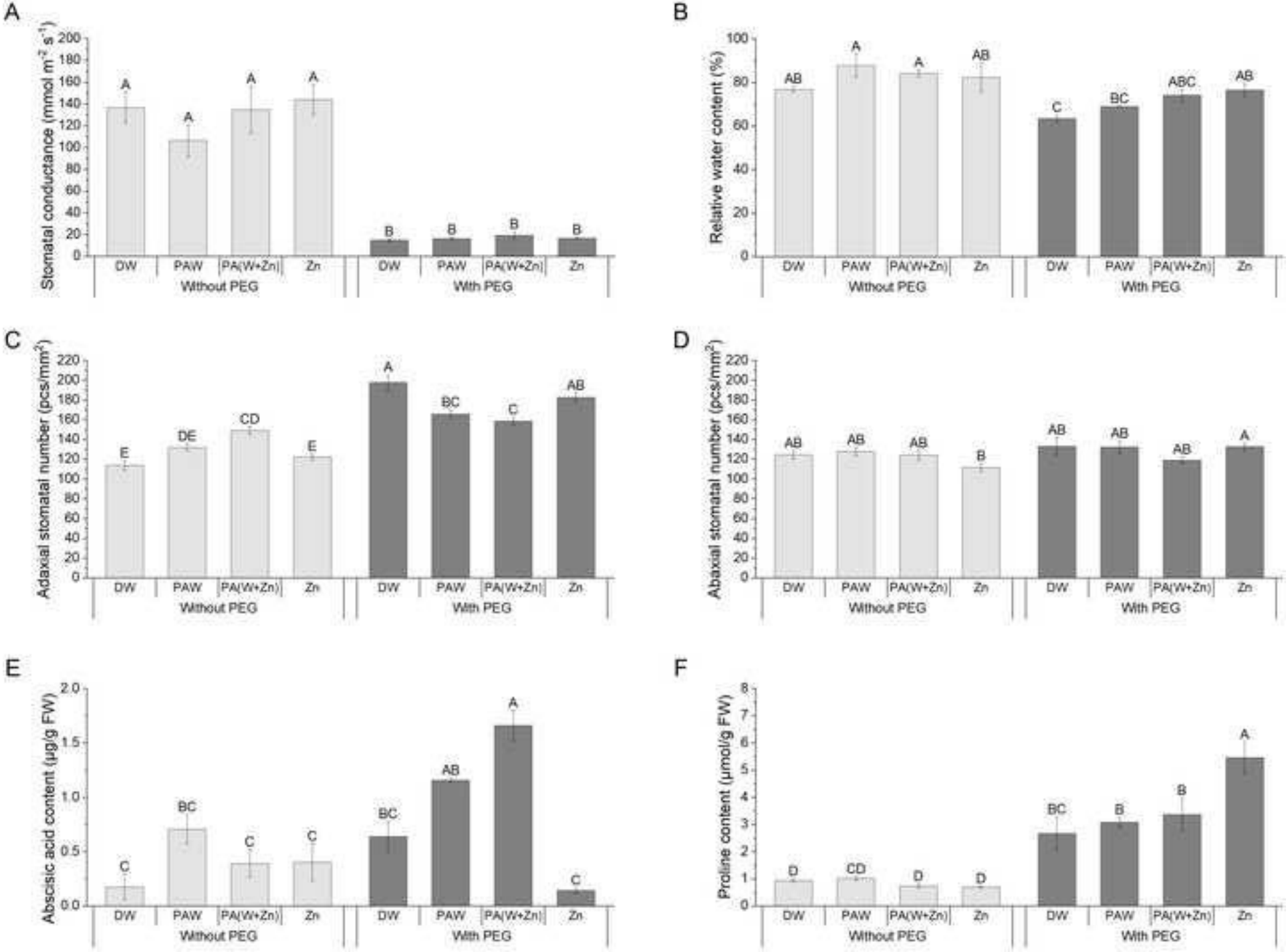
A
Stomatal conductance (mmol m-2 s-1)
0
20
40
60
80
100
120
140
160
180
200
A
A
A
A
B
B
B
B
DW
PAW
PA(W+Zn)
Zn
DW
PAW
PA(W+Zn)
Zn
Without PEG
With PEG
B
Relative water content (%)
0
20
40
60
80
100
AB
A
A
AB
C
BC
ABC
AB
DW
PAW
PA(W+Zn)
Zn
DW
PAW
PA(W+Zn)
Zn
Without PEG
With PEG
C
Adaxial stomatal number (pcs/mm2)
0
20
40
60
80
100
120
140
160
180
200
220
E
DE
CD
E
A
BC
C
AB
DW
PAW
PA(W+Zn)
Zn
DW
PAW
PA(W+Zn)
Zn
Without PEG
With PEG
D
Abaxial stomatal number (pcs/mm2)
0
20
40
60
80
100
120
140
160
180
200
220
AB
AB
AB
B
AB
AB
AB
A
DW
PAW
PA(W+Zn)
Zn
DW
PAW
PA(W+Zn)
Zn
Without PEG
With PEG
E
Abscisic acid content (μg/g FW)
0.0
0.5
1.0
1.5
2.0
C
BC
C
C
BC
AB
A
C
DW
PAW
PA(W+Zn)
Zn
DW
PAW
PA(W+Zn)
Zn
Without PEG
With PEG
F
Proline content (μmol/g FW)
0
1
2
3
4
5
6
7
8
D
CD
D
D
BC
B
B
A
DW
PAW
PA(W+Zn)
Zn
DW
PAW
PA(W+Zn)
Zn
Without PEG
With PEG

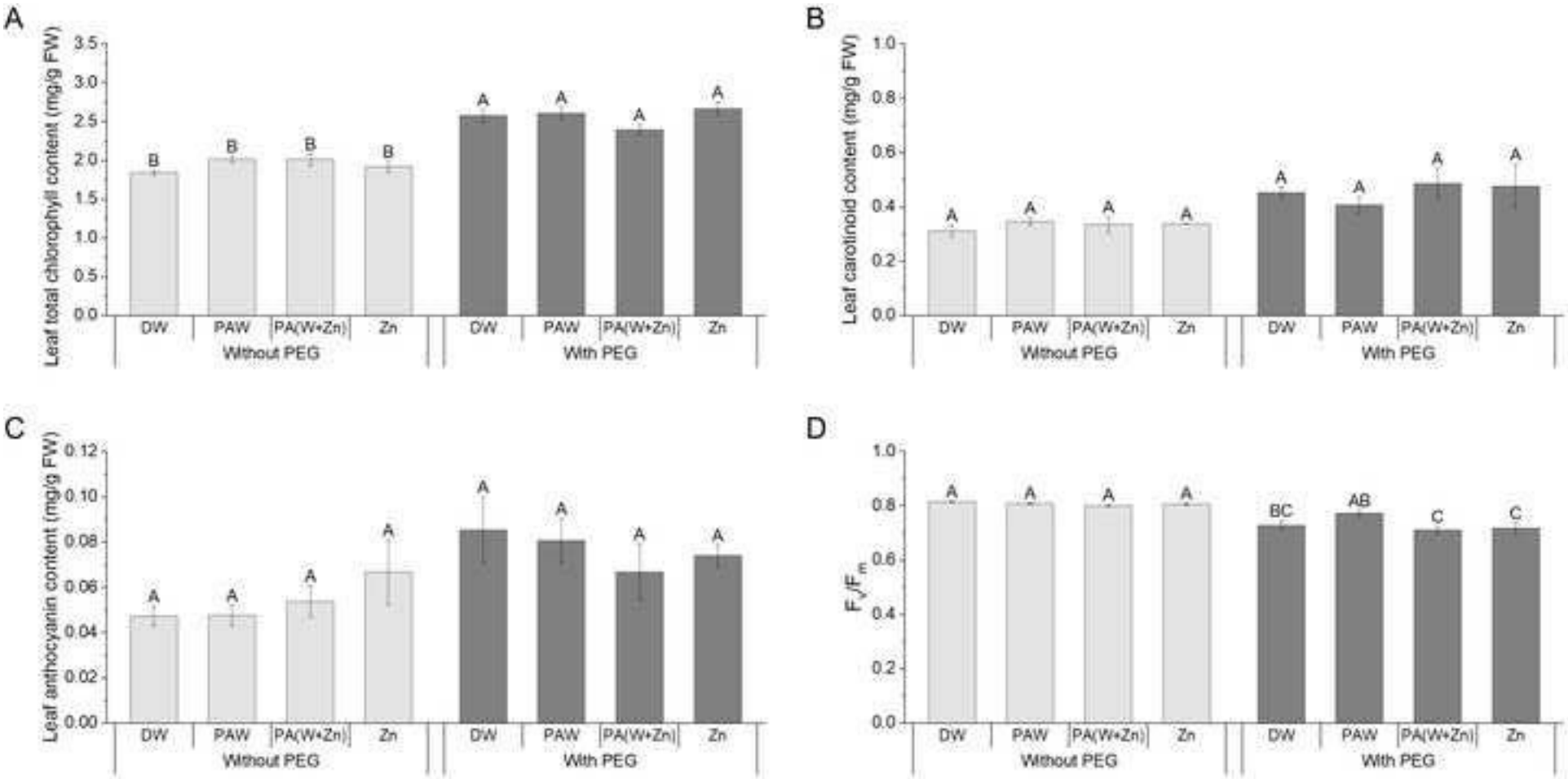
A
Leaf total chlorophyll content (mg/g FW)
3.5
3.0
2.5
2.0
1.5
1.0
0.5
0.0
B
B
B
B
A
A
A
A
DW
PAW
PA(W+Zn)
Zn
DW
PAW
PA(W+Zn)
Zn
Without PEG
With PEG
B
Leaf carotinoid content (mg/g FW)
1.0
0.8
0.6
0.4
0.2
0.0
A
A
A
A
A
A
A
A
DW
PAW
PA(W+Zn)
Zn
DW
PAW
PA(W+Zn)
Zn
Without PEG
With PEG
C
Leaf anthocyanin content (mg/g FW)
0.12
0.10
0.08
0.06
0.04
0.02
0.00
A
A
A
A
A
A
A
A
DW
PAW
PA(W+Zn)
Zn
DW
PAW
PA(W+Zn)
Zn
Without PEG
With PEG
D
F_v/F_m
1.0
0.8
0.6
0.4
0.2
0.0
A
A
A
A
BC
AB
C
C
DW
PAW
PA(W+Zn)
Zn
DW
PAW
PA(W+Zn)
Zn
Without PEG
With PEG

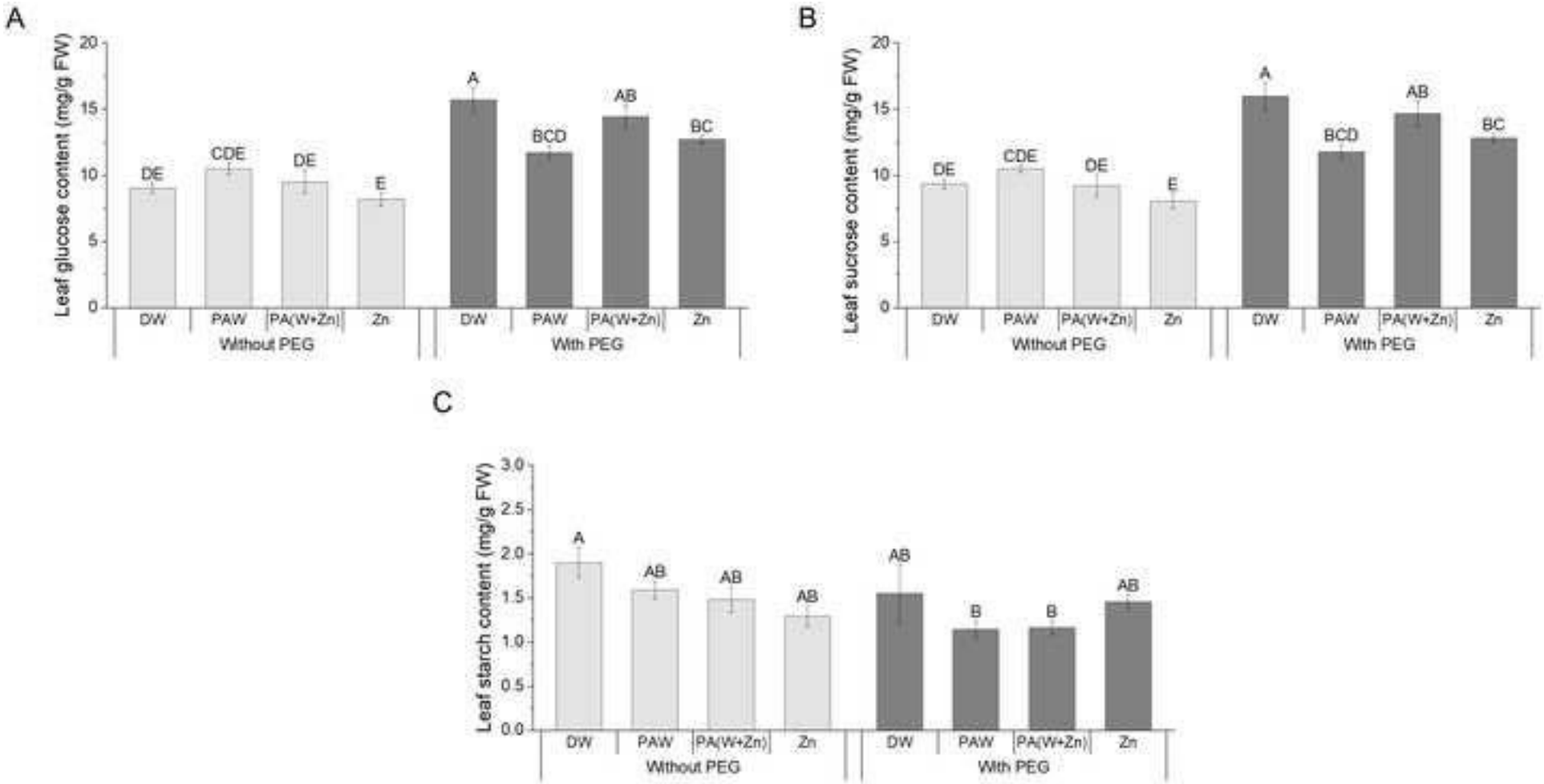
A
Leaf glucose content (mg/g FW)
20
15
10
5
0
DE
CDE
DE
E
A
BCD
AB
BC
DW
PAW
PA(W+Zn)
Zn
Without PEG
With PEG
B
Leaf sucrose content (mg/g FW)
20
15
10
5
0
DE
CDE
DE
E
A
BCD
AB
BC
DW
PAW
PA(W+Zn)
Zn
Without PEG
With PEG
C
Leaf starch content (mg/g FW)
3.0
2.5
2.0
1.5
1.0
0.5
0.0
A
AB
AB
AB
AB
B
B
AB
DW
PAW
PA(W+Zn)
Zn
Without PEG
With PEG

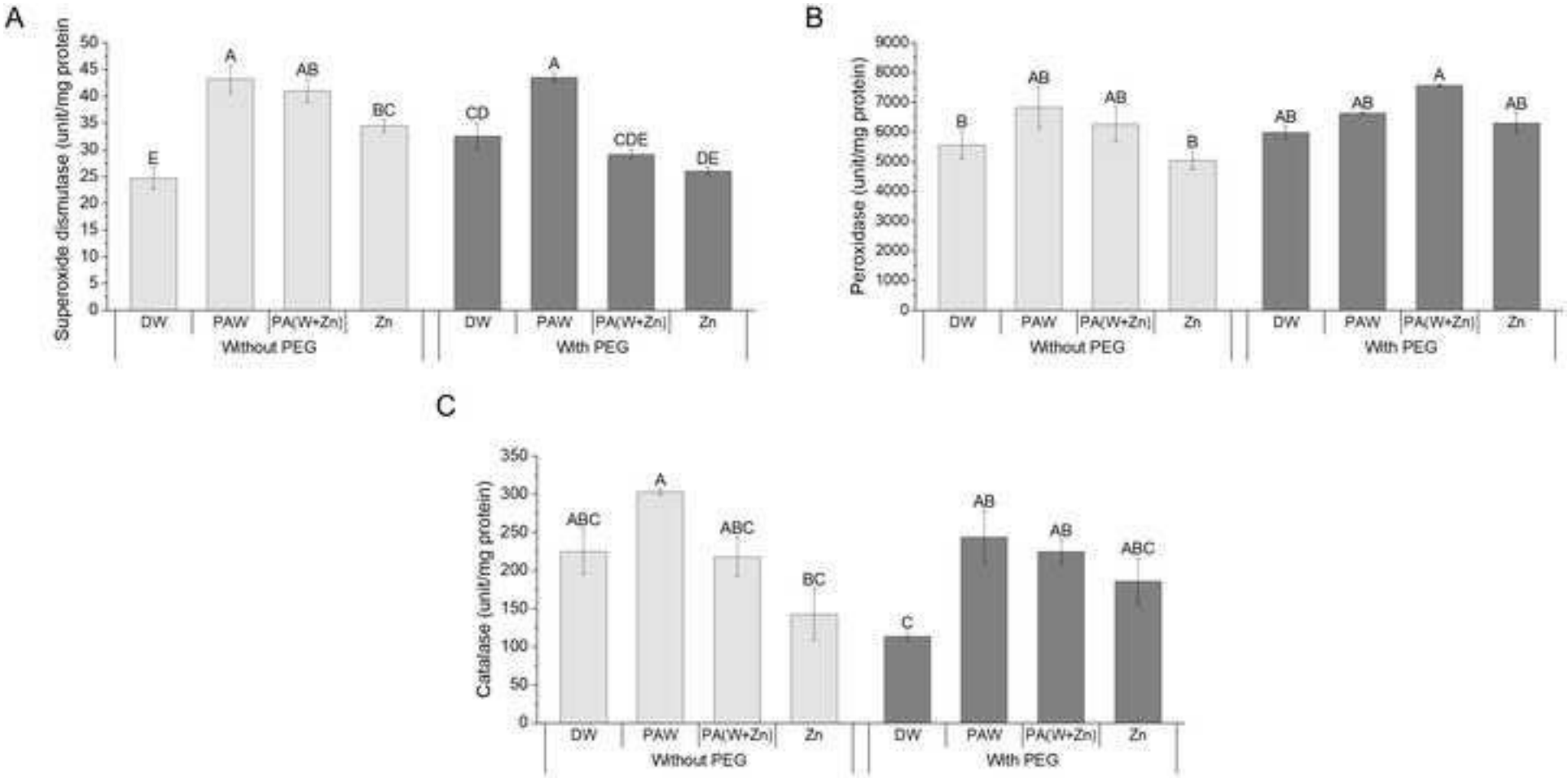
A
Superoxide dismutase (unit/mg protein
50
45
40
35
30
25
20
15
10
5
0
E
A
AB
BC
CD
A
CDE
DE
DW
PAW
PA(W+Zn)
Zn
Without PEG
With PEG
B
Peroxidase (unit/mg protein)
9000
8000
7000
6000
5000
4000
3000
2000
1000
0
B
AB
AB
B
AB
AB
A
AB
C
Catalase (unit/mg protein)
350
300
250
200
150
100
50
0
ABC
A
ABC
BC
C
AB
AB
ABC

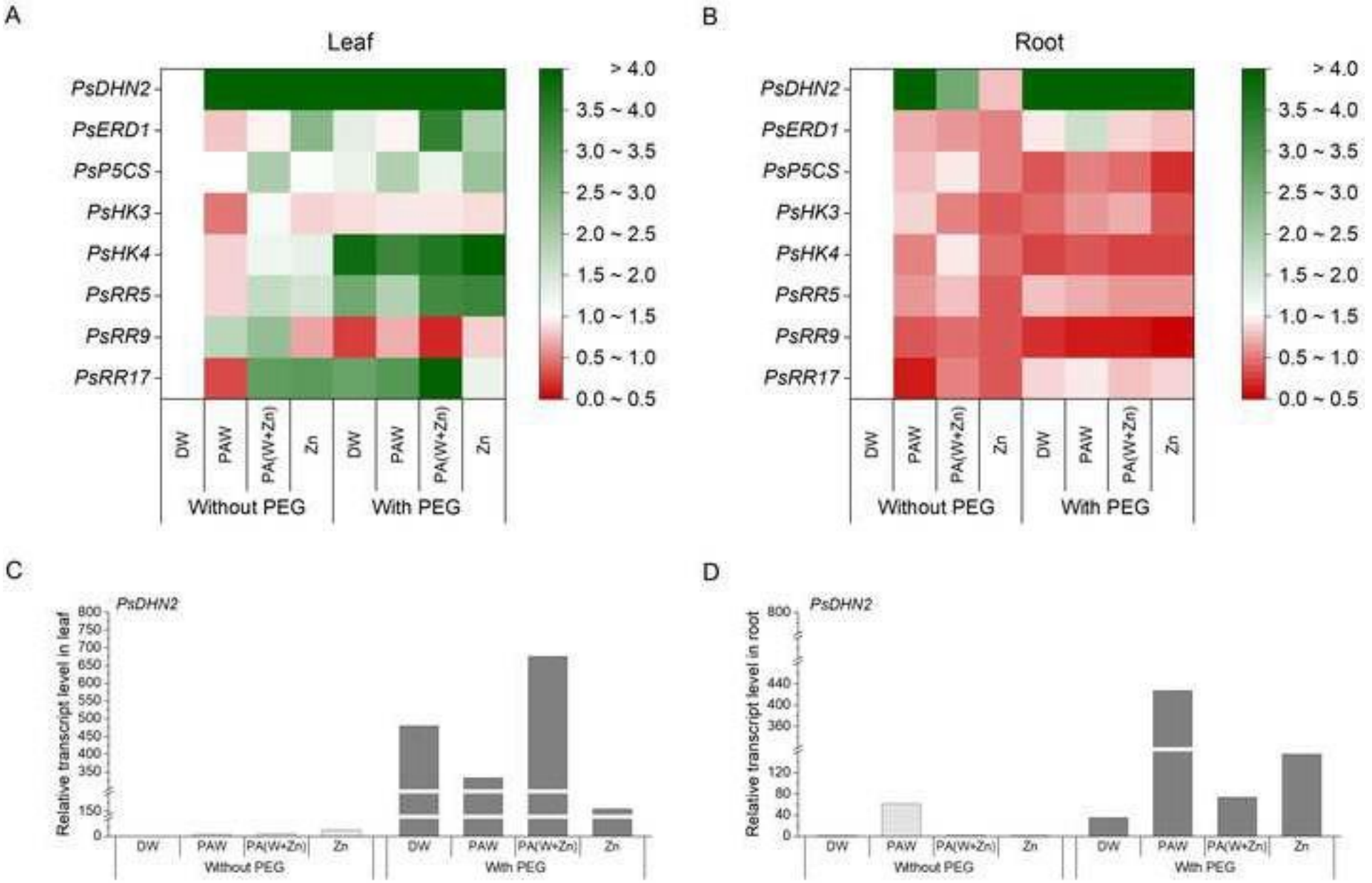
A
Leaf
PsDHN2
PsERD1
PsP5CS
PsHK3
PsHK4
PsRR5
PsRR9
PsRR17
DW
PAW
PA(W+Zn)
Zn
Without PEG
With PEG
> 4.0
3.5 ~ 4.0
3.0 ~ 3.5
2.5 ~ 3.0
2.0 ~ 2.5
1.5 ~ 2.0
1.0 ~ 1.5
0.5 ~ 1.0
0.0 ~ 0.5
B
Root
C
PsDHN2
Relative transcript level in leaf
D
Relative transcript level in root

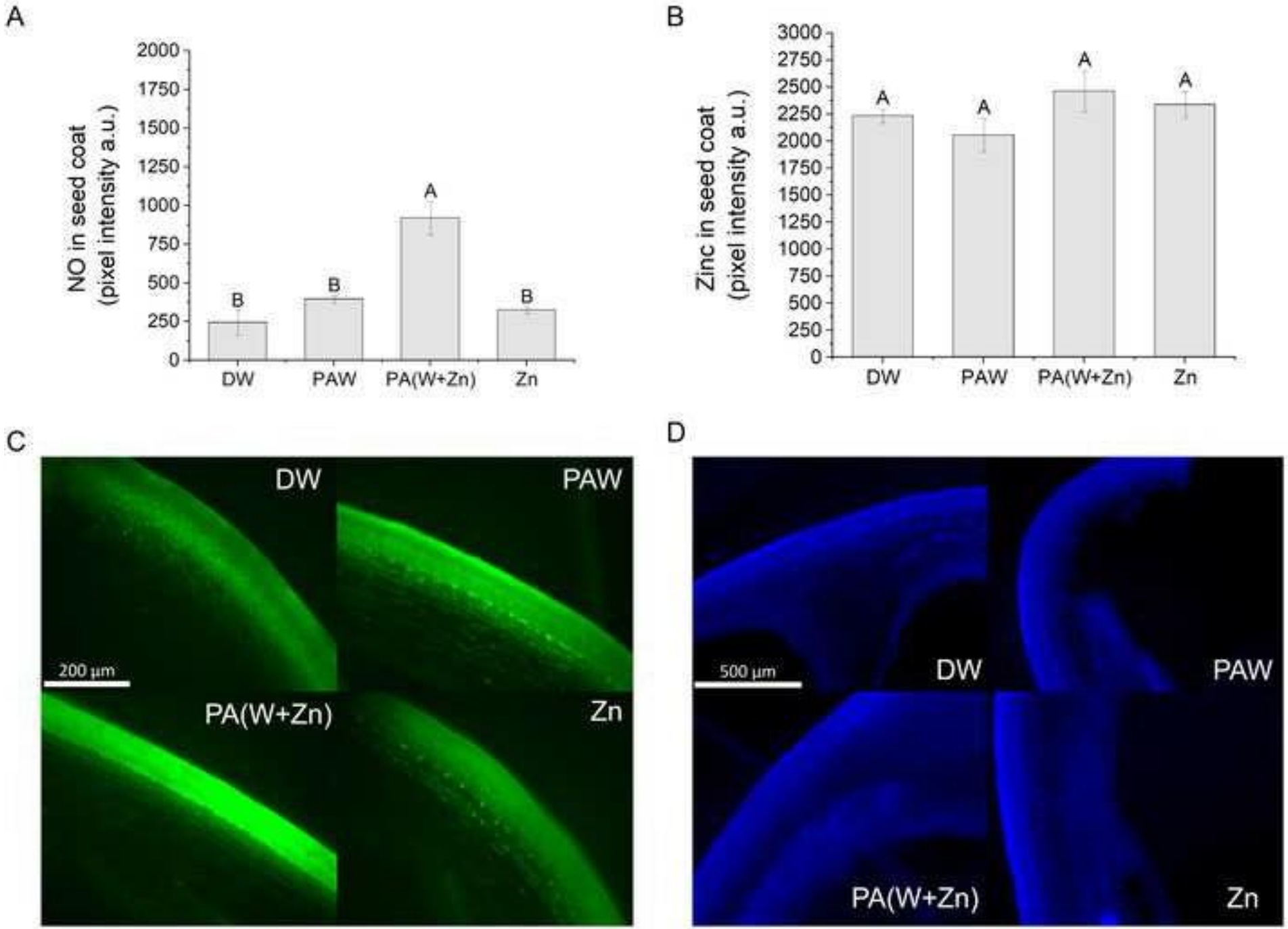
A
NO in seed coat
(pixel intensity a.u.)
2000
1750
1500
1250
1000
750
500
250
0
B
B
A
B
DW
PAW
PA(W+Zn)
Zn
B
Zinc in seed coat
(pixel intensity a.u.)
3000
2750
2500
2250
2000
1750
1500
1250
1000
750
500
250
0
A
A
A
A
DW
PAW
PA(W+Zn)
Zn
C
DW
PAW
200 µm
PA(W+Zn)
Zn
D
500 µm
DW
PAW
PA(W+Zn)
Zn